論文 / 著書情報
Article / Book Information

題目(和文)	超臨界二酸化炭素エマルジョンを用いたNi-Pの無電解析出
Title(English)	Electroless Ni-P deposition using supercritical carbon dioxide emulsion
著者(和文)	内山浩幹
Author(English)	Hiroki Uchiyama
出典(和文)	学位:博士(工学), 学位授与機関:東京工業大学, 報告番号:甲第8771号, 授与年月日:2012年3月26日, 学位の種別:課程博士, 審査員:曽根 正人
Citation(English)	Degree:Doctor (Engineering), Conferring organization: Tokyo Institute of Technology, Report number:甲第8771号, Conferred date:2012/3/26, Degree Type:Course doctor, Examiner:
学位種別(和文)	博士論文
Type(English)	Doctoral Thesis

Electroless Ni-P Deposition Using Supercritical Carbon Dioxide Emulsion

Doctor of Engineering

Department of Materials Science and Engineering

Tokyo Institute of Technology

Hiroki Uchiyama

2012

TABLE OF CONTENTS

CHAPTER 1

Introduction

1. 1. Three-Dimensional Integration Technology

A traditional integrated circuit (IC) is fabricated on a single flat silicon wafer restricted to a two-dimensional (2D) architecture. With the development of microelectronic technologies in recent decades, improved performance, smaller form factors, and lower-cost electronic products have all become basic requirements for surviving in the market. Yet in place of traditional ICs, these needs can only be satisfied by what we call three-dimensional (3D) integration technology (Fig. 1.1).[1-4] This is a technology for vertically stacking and interconnecting multiple components in order to build advanced integrated circuits. The stacking of multiple materials, technologies, and functional components such as complementary metal-oxide-semiconductor (CMOS) devices and microelectromechanical systems (MEMS) in these integrated 3D systems enables both heterogeneous integration and high functionality.

Most MEMS devices can be broadly divided into two categories: passive

devices such as sensors and active devices such as actuators.[1-5] Examples of MEMS sensors include pressure sensors, optical sensors, accelerometers, gyroscopes, chemical sensors, and energy-scavenging devices. Examples of MEMS actuators include heating elements, micromirrors, resonators, mechanical motion devices, switches, and micropumps. Techniques for microfabrication and the still smaller nanofabrication are now used to fabricate complex 3D micro/nanostructures. As an example of the gyroscope chip, the monocrystalline silicon capacitive gyroscope sensor and parts of the gyroscope package are pre-fabricated together and then bonded to the top CMOS Al metal layer of a CMOS IC wafer with an etched cavity using an Al/Ge eutectic bonding process. Figs. 1.2 (a) and 1.2 (b) respectively show a cross-sectional image and top view of a commercial gyroscope.[5] Figs. 1.3 (a) and 1.3 (b) show a SEM image of a piston-type monocrystalline silicon micromirror array and an example of a detailed process flow for the integration of the micromirror array, respectively.[5]

1. 2. Thin-Film Formation Technology

Thin-film formation technology is a major research area. This technology has evolved through the development of materials for applications in microelectronics, optics, and nano-technology.[6-9] The key processes for thin film formation have been either chemical or physical so far, but combinations of these with various other processes are being increasingly applied. Thin film deposition technology can be classified into two types: those that rely on chemical reactions and those that rely on physical reactions.[6-11] Chemical vapor deposition (CVD), atomic layer deposition (ALD), electrochemical deposition, and epitaxy are examples of the former. These processes exploit the creation of solid materials directly from chemical reactions in gas and/or liquid compositions or reactions with substrate materials. Physical vapor deposition (PVD), evaporation, and sputtering are examples of physical deposition techniques. In all of these physical processes, the deposited material is moved onto the substrate physically.

The main vapor deposition technologies are PVD and CVD.[6-8] PVD encompasses a number of deposition technologies in which material is released from a source and transferred to a substrate. PVD employs standard technologies for depositing metals. The technique is far more common than CVD for metals, as it can be performed at lower process risk and incurs much

lower cost for materials. Yet PVD films are inferior in quality to CVD films. More specifically, they have higher resistivity, more defects and traps for insulators, and inferior step coverage. CVD processes are ideal when the design target is a thin film with good step coverage. Various materials can be deposited with CVD technology. The Low-Pressure CVD (LPCVD) process produces layers with highly uniform thickness and material characteristics. The main demerits of LPCVD are a high deposition temperature and a relatively slow deposition rate. Plasma Enhanced CVD (PECVD) can be performed at lower temperatures, thanks to the extra energy the gas molecules receive from the plasma in the reactor. Yet PECVD films tend to be inferior in quality to films produced from processes running at higher temperatures.

There are also methods of liquid phase deposition, such as conventional plating, the sol-gel process, the coating method, and the like.[6,7,9] Compared to gas phase methods, liquid phase deposition offers advantages such as low-temperature film formation, low cost, and simple film-forming processes.

Electrochemical deposition, the basic technology covered in this paper, is explained a few pages later in section 1.3

The current MEMS have basically been developed by the same process used to fabricate semiconductors.[5,12] Without question, the thin-film formation technology remains a vital element in these fields. Yet the growing complexity

and shrinking dimensions of microelectronics nowadays are placing stringent demands on this technology, and these demands have yet to be fully satisfied.[1-5,12-15] Thin films with extremely few defects are mandatory. Fig. 1.4 shows examples of the types of defects to be avoided.[6-9,16-21] While the causes of these defects differ, no thin-film formation technology is immune to them. Non-conformal growths such as nodules, and defects in film coverage such as pits and pinholes, are inescapable. The conventional thin-film formation technology is incapable of easily controlling them across the board. These defects compromise the properties of the film, and their influence grows in a stacking structure such as a 3D IC or MEMS. The defects on a film worsen the properties of another film formed directly on top. The formation of subsequent layers over the defect in this fashion ultimately results in an imperfect structure such as that shown in Fig. 1.5 (a).[22] The illustrations in Fig. 1.5 compare planarized and non-planarized surface topographies of a multilayer interconnect. As this comparison shows, a technology capable of forming smooth, uniform thin films with few micro- or nano-size defects will be indispensable for the 3D integration technology of the future.

1. 3. Electrochemical Deposition

As devices get progressively smaller, accommodated by scaling and material changes, the CVD and ALD techniques are expected to surmount the challenges now confronting them.[11,23] The challenges confronting CVD are a high processing temperature and the low transportation density of the organometallic compounds. ALD, meanwhile, is slow in depositing films and requires the use of special organometallic compounds. As added drawbacks, both methods are expensive and involve very complicated fabrication processes. Electrochemical deposition, on the other hand, offers many promising advantages such as good uniformity and gap-filling ability, selectivity, low processing temperatures, and simple operation. High-performance thin films can now be fabricated by electrochemical deposition, and thin film formation by electrochemical processes will be employed for the fabrication of the 3D integrated device. The 3D integrated device has made stride after stride through the successive development of innovative technologies such as the damascene process (Fig. 1.6).[12]

Electrochemical processes for thin film formation are classified into two types, namely, electrodeposition (electroplating (EP)) and electroless deposition (electroless plating (ELP)).[7,9] The diagrams in Fig. 1.7 illustrate the electrochemical deposition processes.[9] EP uses the substrate as a cathode

immersed in an aqueous solution of an electrolyte. The metal ions are deposited directly onto the substrate. Only some metallic elements, alloys, and oxides are actually deposited for commercial applications. The films can be formed in any thickness, from less than 1 μm to several hundreds of μm. The deposition is best controlled when the system employs an external electrical potential, but electrical contact with the substrate is required when the substrate is immersed in the liquid bath. In any process, the surface of the substrate must have an electrically conducting coating before the deposition can be take place. In ELP, metallic coatings are formed as a result of a chemical reaction between the reducing agent present in the solution and the metal ions. The chemical process can only be localized on a particular surface when the surface itself serves as a catalyst. When the catalyst itself is a reducing agent, autocatalysis and the deposition of coatings of theoretically unlimited thickness are assured. Autocatalytic reactions of this type constitute the essence of the practical processes of ELP. This is why these plating processes are sometimes called autocatalytic. ELP offers the following advantages over similar electrochemical methods:[7,24,25]

1. The coatings can be deposited on electrically nonconductive materials (on almost any surface that remains stable in the ELP solution).
2. The coatings have more uniform thickness, irrespective of the shape of the

product plated (Fig. 1.8).[25]

3. The deposition is simple: immersing the pretreated product in the ELP solution is enough.
4. Coatings with unique mechanical, magnetic, and chemical properties can be formed.

Compared with EP, the ELP technique generates far fewer defects and forms much thinner films. These advantages heighten the expectations of ELP for 3D integration technology.

Cu is the interconnect material of choice in the metallization step for advanced semiconductor device manufacturing.[6,9] Four different approaches can now be used for Cu metallization: PVD, CVD, EP, or ELP.[6,9,26,27] The main technique for Cu metallization in ICs at present is EP. Yet as the width of interconnects narrows and the aspect ratio grows, the depletion of active ions makes it difficult to plate void-free copper in submicrometer trenches or vias.[28] In plating, cupric ions are reduced to copper in the trenches or vias. Because the cupric ions deposit on the surface more quickly than they diffuse from the bulk solution into the bottom of trenches or vias, the concentration of cupric ions at the bottom is lower than that at the top. This concentration gradient leads to a difference in deposition rates, namely, a faster deposition rate at the top than that at the bottom. Eventually, voids form inside. The need for applied power

and nonuniform current distribution in EP has diverted the emphasis to alternatives, namely, ELP and pulse electroplating (Pulse-EP), in the development of future 3D integration technology.[29,30] Pulse-EP, a technique with multiple process parameters and a higher instantaneous current density than direct current electroplating (dc-EP), is widely recognized as an important technology for improving the properties of deposits.[31,32] Pulse-EP has a periodic relaxation time during which reactant can be supplied from the bulk solution to reduce the concentration differential. The high-frequency pulses enhance mass transport, which renders more uniform deposition and void-free deposits. Fig. 1.9 shows typical results.[33] The dc-EP clearly obtains abnormal growth on the Cu wire shown in Fig. 1.9 (a), while pulse-EP obtains a smooth deposition on the wire shown in Fig. 1.9 (b).

Investigators in the field have cited two advantages of pulse-EP.[31,32] First, a higher average cathodic current density for deposition can be applied to the plating system. While the theoretical limiting current density may be a constant under both dc and pulse plating, the practical current limit for a pulse current can far exceed that for dc-EP. Second, a pulse-EP can obtain a fine-grained deposit. The desired properties can be realized by adjusting the on-time, off-time, and current density of the pulse current.

Anomalies such as nodules, pits, and pinholes are common to most plating

technologies.[9,20,24,25] To reduce the influence of pinholes and other through-holes in EP, the film thickness is increased to tens of micrometers or over. This increased thickness has downsides, however. In addition to requiring more material, thicker films permit increases in unusual growth portions such as nodules, both in size and in number. They are also more difficult to form within minute areas. When, on the other hand, a film is thinner than before, nodule and pinhole defects are difficult to control simultaneously. As mentioned above, the films formed by ELP are thinner and have fewer defects than the films formed by EP. Yet to produce ever-more minute structures such as electronic device, nodules and pinholes must both be suppressed.

1. 4. Supercritical Fluid Technology

A fluid is said to be ‘supercritical’ when its temperature and pressure exceed the critical temperature (T_c) and pressure (P_c). Fig. 1.10 is a pressure-temperature diagram for a pure substance.[34] The density, viscosity, and diffusivity of a supercritical fluid (SCF) are intermediate between those of liquids and gases. Moreover, these properties can be continuously adjusted from gas to liquid phases with small pressure and temperature variations, as shown in Fig. 1.11. Processes using these fluids are of great value in many fields, from analytical and preparative separations to organic and inorganic synthesis, waste

management, and material processing (nanomaterials, nanostructured materials, thin films, coating).[34-38] Carbon dioxide (CO_2) has become one of the most extensively used SCFs, by dint of its relatively low critical temperature and pressure (T_c = 304 K, P_c = 7.4 MPa). The low T_c of CO_2 makes it especially attractive for processing heat-sensitive products. CO_2 has the further advantage of being an inexpensive, non-toxic, non-flammable, and easily recyclable solvent.

When the medium used for fabricating a microstructure by thin-film formation technology is the gas phase, the low solubility of the materials to the medium make it difficult to deposit a minute structure uniformly. When, on the other hand, the medium is the liquid phase, the high viscosity makes it difficult to deposit a film that conforms closely to an intricate microstructure. To surmount these problems, an SCF-assisted thin-film formation technology with outstanding characteristics has been developed in recent years.

SCF-assisted techniques of thin film production can be divided in two groups:

- physical deposition processes
- chemical deposition processes

Physical film deposition processes are related to the RESS (Rapid Expansion of a Supercritical Solution) process and its modifications. The RESS

process was first proposed by Matson et al.[39] The diagram in Fig. 1.12 illustrates the RESS process. The underlying concept is simple: when RESS products are sprayed onto a solid substrate, films can be formed. Petersen et al.[40] used this technique to form amorphous powders and thin films from organic and inorganic materials. SiO_2 films with a uniform thickness of about 1 μm were deposited on a Millipore filter.

Meanwhile, Sievers and coworkers proposed a film deposition process by a chemical reaction in SCF .[41-43] In essence, they proposed a RESS process where a chemical reaction is induced when the SCF solution expands, and where a film of the desired material forms from the chemical reaction deposits on the substrate surface. While the film thickness attainable by this technique has not been described, this parameter can be controlled by adjusting the expansion time. Louchev et al.[44] used resistive or laser heating to decompose a precursor compound that had been previously dissolved in an SCF. Operating in this manner, they produced thin films of Cu with thicknesses as low as 50 nm. Various scientific papers have described an SCF alternative to CVD, a process Watkins et al. called “chemical fluid deposition” (CFD).[45-47] The illustration in Fig. 1.13 is a schematic of a cold wall CFD reactor. Watkins et al. described the formation of copper and nickel films on silicon wafers and patterned Si wafers. The SEM images in Figs. 1.14 (a) and (b) respectively show an Ni film

deposited on a Si wafer with a spherical morphology and grain sizes of 80-190 nm, and a highly conformal Ni film deposited onto a patterned Si wafer.[46,47]

Sone et al. proposed another thin film deposition technique, a variation of the traditional hexane emulsion electroplating method.[48-51] They induced a supercritical carbon dioxide (sc-CO_2) electroplating reaction in an emulsion of dense CO_2, a metal salt solution (the electroplating solution), and a surfactant with agitation in a high-pressure cell operated at 100 bar. When Yan et al. compared the electrochemical properties of hexane and dense CO_2 emulsions, they found them to be very similar. Next, in electro-deposition experiments using sc-CO_2, they obtained nickel nanostructured surfaces with higher uniformity, higher hardness, and smoother formability than could be obtained using the liquid process. They attributed the absence of surface defects in their films to two properties, namely, the high solubility of the hydrogen (produced during the reaction) in the sc-CO_2 and the reduced viscosity of the sc-CO_2. These properties greatly reduce surface imperfections by eliminating obstacles and assuring fast contact between the deposition material and the surface to be covered.

1. 5. Object of This Thesis

The miniaturization and sophistication of electronic devices have been advancing remarkably. The films to be incorporated into the coming 3D integration technology are expected to have fewer defects and more perfect flatness than before. The development of a film formation technology that inherits the excellent properties of ELP and reliably controls defects is clearly in need. This paper proposes a novel ELP technique that brings together SCF and ELP technologies with excellent results. It discusses the characteristic of metal films fabricated by this technique, and the mechanism by which the technique suppresses defects such nodules and pinholes. We call this technology the ELP-SCE (electroless plating using a supercritical carbon dioxide emulsion).

In Chapter 2 we discuss studies of the fundamental film formation conditions of this novel ELP-SCE method, as well as the surface morphology of films formed by the method. We closely examine whether films produced by ELP-SCE form nodule and pinhole defects of microscopically observable sizes. To clearly show the difference between ELP-SCE and the conventional method, we fabricated plating films by each method using the same substrate, pretreatment, and ELP solution composition, then compared the surface morphologies of the fabricated films.

In Chapter 3 we discuss the defect-suppression mechanism of ELP-SCE from a macroscopic viewpoint. ELP-SCE formed a high-quality film free from nodules and pinholes. We explain how ELP-SCE suppresses defects by referring to the factors that influence surface formation with the conventional plating technology. The stirring speed, additive, and dissolved oxygen and pH in the solution all affect the surface morphology of the plating film formed by the conventional method. In ELP-SCE we add a nonionic surfactant and high-speed stirring, in order to emulsify the dense CO_2 and plating solution. This emulsification is effective in reducing both the dissolved oxygen and pH in the plating solution. By combining the conditions of ELP-SCE with the conventional plating conditions that permit nodule formulation, we were able to identify and study the factors affecting nodule formation.

In Chapter 4 we discuss the defect-suppression mechanism of ELP-SCE from a microscopic viewpoint. By directly observing how ELP-SCE influences minute convex structures such as nodules, we can more clearly understand the defect-suppression mechanism of ELP-SCE. We prepared plated films with nodules and then re-plated them by ELP-SCE and conventional methods in order to directly observe the changes of the surface morphologies. By doing so, we developed an observation technique capable of identifying specific nodules

before and after re-plating.

The main purposes of the research for this thesis are to develop an innovative thin-film formation method capable of forming films with high surface flatness and few defects, and to elucidate the basic properties of this novel method and the mechanism by which the method suppresses defects such as nodules and pinholes.

References

1. X. Gagnard and T. Mourier, *Microelectron. Eng.*, **87**, 470 (2010).
2. T. Tekin, *IEEE J. Sel. Top. Quant. Electron.*, **17**, 704 (2011).
3. B. Bhushan, *Microelectron. Eng.*, **84**, 387 (2007).
4. K. W. Lee, A. Noriki, K. Kiyoyama, T. Fukushima, T. Tanaka, and M. Koyanagi, *IEEE Trans. Electron dev.*, **58**, 748 (2011).
5. M. Lapisa and G. Stemme, *IEEE J. Sel. Top. Quant. Electron.,* **17**, 629 (2011).
6. L. B. Freund and S. Suresh, *Thin Film Materials*., Cambridge University Press, Cambridge (2009).
7. A. A. Tracton, *Coatings Technology Handbook*, 3nd ed., CRC Press Taylor & Francis Group, New York (2006).
8. D. M. Dobkin and M. K. Zuraw, *Principles of Chemical Vapor Deposition*., Kluwer Academic Publishers, Dordrecht (2010).
9. M. Paunovic and M. Schlesinger, *Fundamentals of Electrochemical Deposition*, 2nd ed., John Wiley & Sons, Hoboken, NJ (2006).
10. M. Leskela and M. Ritalla, *Thin Solid Films,* **409**, 138 (2002),
11. B. S. Lim, A. Rahtu, and R. G. Gordon, *Nat. Mater.*, **2**, 749 (2003).
12. P. C. Andricacos, C. Uzoh, J. O. Dukovic, J. Horkans, and H. Deligianni, *IBM J. Res. Dev.*, **42**, 567 (1998).

13. J. W. Schultze and A. Bressel, *Electrochim. Acta*, **47**, 3 (2001).

14. H. Honma, *Electrochim. Acta*, **47**, 75 (2001).

15. F. Formanek, N. Takeyasu, T. Tanaka, K. Chiyoda, A. Ishikawa, and S. Kawata, *Appl. Phys. Lett*., **88**, 083110 (2006).

16. S. Y. Chang, C. J. Hsu, R. H. Fang, and S. J. Lin, *J. Electrochem. Soc*., **150**, C603 (2003).

17. T. Tsunoda, H. Nagashima, H. Nishinakayama, H. Watanabe, and H. Honma, *Hyomen Gijutsu*, **56**, 463 (2005).

18. H. H. Hsu, J. W. Yeh, and S. J. Lin, *J. Electrochem. Soc.*, **150**, C813 (2003).

19. H. Yoshida, M. Sone, H. Wakabayashi, H. Yan, K. Abe, X. T. Tao, A. Mizushima, S. Ichihara, and S. Myata, *Thin Solid Films*, **446**, 194 (2004).

20. Y. Nakamaru, T. Joya, K. Tashiro, and H. Honma, *Hyomen Gijutsu*, **60**, 661 (2009).

21. D. G. Stearns, P. B. Mirkarimi, and E. Spiller, *Thin Solid Films*, **446**, 37 (2004).

22. P. B. Zantye, A. Kumar, and A. K. Sikder, *Mater. Sci. Eng. R. Rep*., **45**, 89 (2004).

23. E. T. Hunde and J. J. Watkins, *Chem. Mater.*, **16**, 498 (2004).

24. G. O. Malloy and J. B. Hajdu, *Electroless Plating: Fundamentals and Applications*, American Electroplaters and Surface Finishers Society,

Orlando, FL (1990).

25. W. Sha, X. Wu and K. G. Keong, *Electroless Copper and Nickel-phosphorus Plating: Processing, Characterization and Modeling*, Woodhead Publishing, Cambridge, (2011).

26. M. Murakami, M. Moriyama, S. Tsukimoto, and K. Ito, *Hyomen Gijutsu*, **56**, 802 (2005).

27. A. Radisic, O. Luhn, H. G. G. Philipsen, Z. El-Mekki, M. Honore, S. Rodet, S. Armini, C. Drijbooms, H. Bender, and W. Ruythooren, *Microelectron. Eng.*, **88**, 701 (2011).

28. W. C. tsai, C. C. Wan, and Y. Y. Wang, *J. Electrochem. Soc.*, **149**, C229 (2002).

29. L. Hofmann, R. Ecke, S. E. Schulz, and T. Gessner, *Microelectron. Eng.*, **88**, 705 (2011).

30. S. Armini and A. M. Caro, *J. Electrochem. Soc.*, **157**, D74 (2010).

31. I. Ohno, *J. Met. Finish. Soc. Jpn.,* **39**, 149 (1988).

32. M. S. Chandrasekar and M. Pushpavanam, *Electrochim. Acta.*, **53**, 3313 (2008).

33. A. R. Despic and K. I. Popov, *J. Appl. Electrochem.*, **1**, 275 (1971).

34. J.A. Darr and M. Poliakoff, *Chem. Rev.*, **99**, 495 (1999).

35. E. Reverchon and R. Adami, *J. Supercrit. Fluids.*, **37**, 1 (2006).

36. M. Mchugh and V. Krukonis, *Supercritical Fluid Extraction*, Butterworth-Heinemann, Boston, (1994).

37. E.J. Beckman, *J. Supercrit. Fluids.*, **28**, 121 (2004).

38. T. Ajiri, *Nano technology with Supercritical Fluids*, CMC Publishing, Japan, (2010).

39. D.W. Matson, J.L. Fulton, R.C. Petersen, and R.D. Smith, *Ind. Eng. Chem Res.*, **26**, 2298. (1987).

40. R.C. Petersen, D.W. Matson, and R.D. Smith, *J. Am. Chem. Soc.*, **108**, 2100 (1986).

41. B.N.H. R.E. Sievers, *Chemical deposition using supercritical solution*. 1990: USA.

42. B.M. Hybertson, B.N. Hansen, R.M. Barkley, and R.E. Sievers, *Mater. Res. Bull.,* **26**, 1127 (1991).

43. B.N. Hansen, B.M. Hybertson, R.M. Barkley, and R.E. Sievers, *Chem. Mater.,* **4**, 749 (1992).

44. O.A. Louchev, V.K. Popov, and E.N. Antonov, *J. Crystal Growth*, **155**, 276 (1995).

45. A. H. Romang and J. J. Watkins, *Chem. Rev.*, **110**, 459 (2010).

46. J. M. Blackburn, D. P. Long, A. Cabanas, and J. J. Watkins, *Science*, **294**, 141 (2001).

47. E. T. Hunde and J. J. Watkins, *Chem. Mater.,* **16**, 498 (2004).

48. H. Yoshida, M. Sone, A. Mizushima, K. Abe, X.T. Tao, S. Ichihara, and S. Miyata, *Chem. Lett.*, 1086 (2002).

49. H. Yoshida, M. Sone, A. Mizushiama, H. Yan, H. Wakabayashi, K. Abe, X. T. Tao, S. Ichihara, and S. Miyata, *Surf. Coating. Tech.*, **173**, 285 (2003).

50. H. Yan, M. Sone, A. Mizushima, T. Nagai, K. Abe, S. Ichihara, and S. Miyata, *Surf. Coating. Tech.*, **187**, 86 (2004).

51. H. Yoshida, M. Sone, H. Wakabayashi, H. Yan, K. Abe, X. T. Tao, A. Mizushiama, S. Ichihara, and S. Miyata, *Surf. Coating. Tech.*, **446**, 194 (2004).

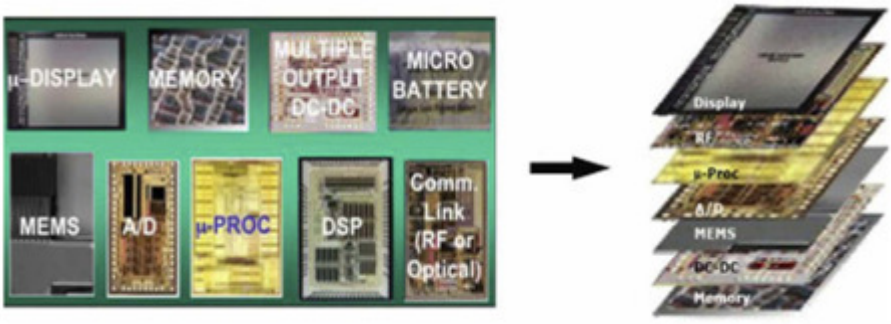

Fig. 1.1 3D integration, heterogeneous integration, the bonding of disparate technologies and functionalities to fabricate a compacted device.[1]

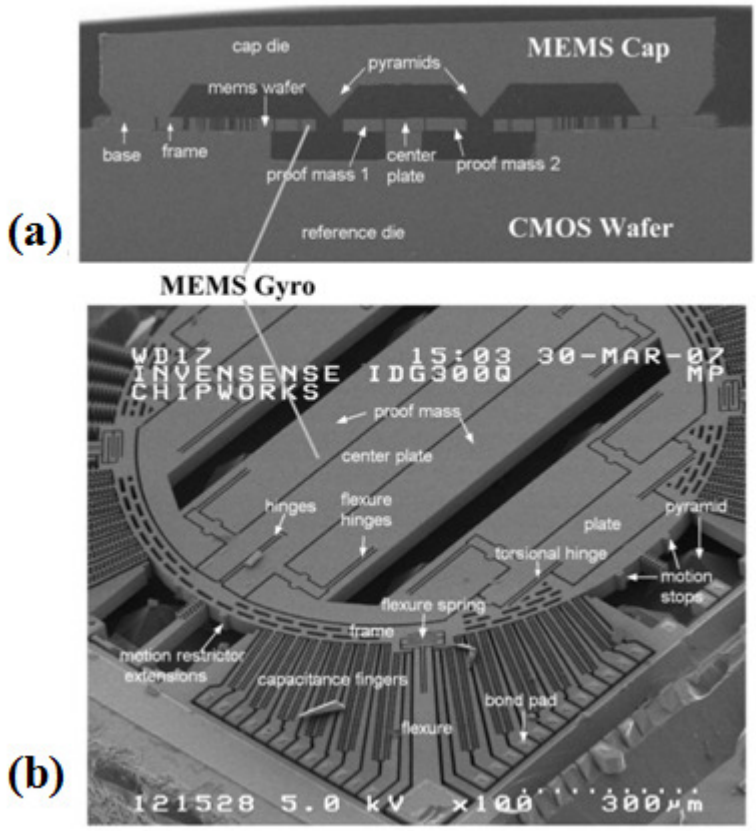

Fig. 1.2 Commercially available gyroscope integrated with CMOS ICs.[5]

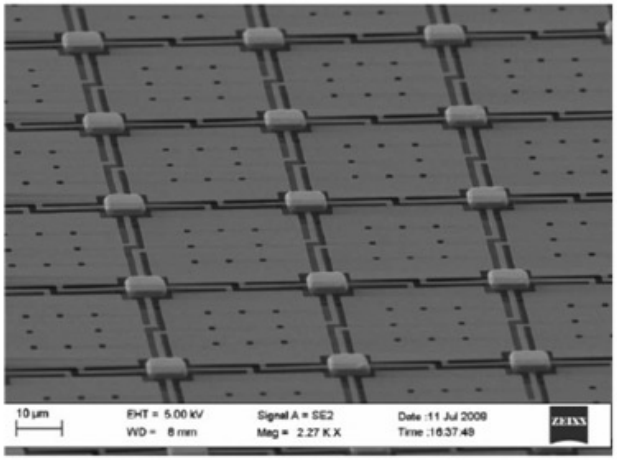

(a)

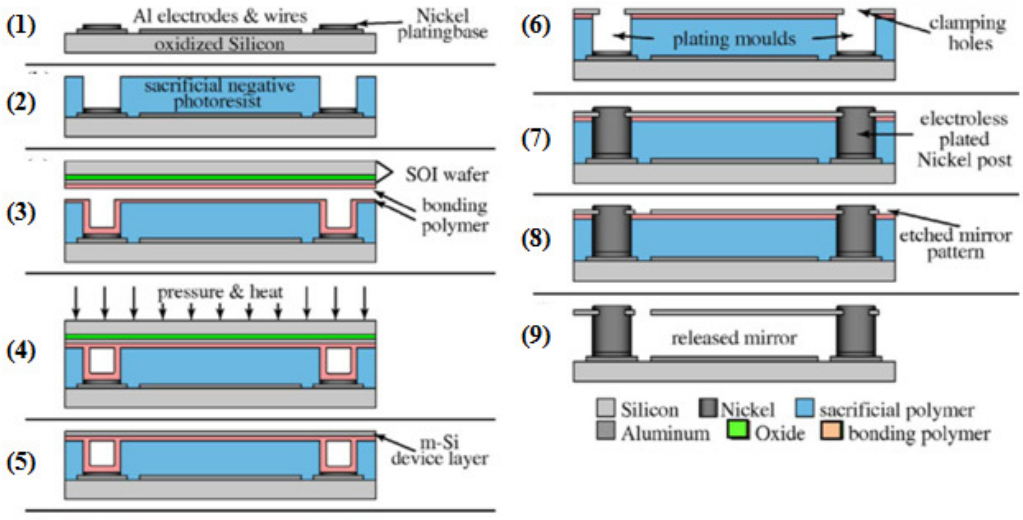

(b)

Fig. 1.3 (a) piston-type monocrystalline silicon mirror array manufactures with the process shown in (b) heterogeneous integration process.[5]

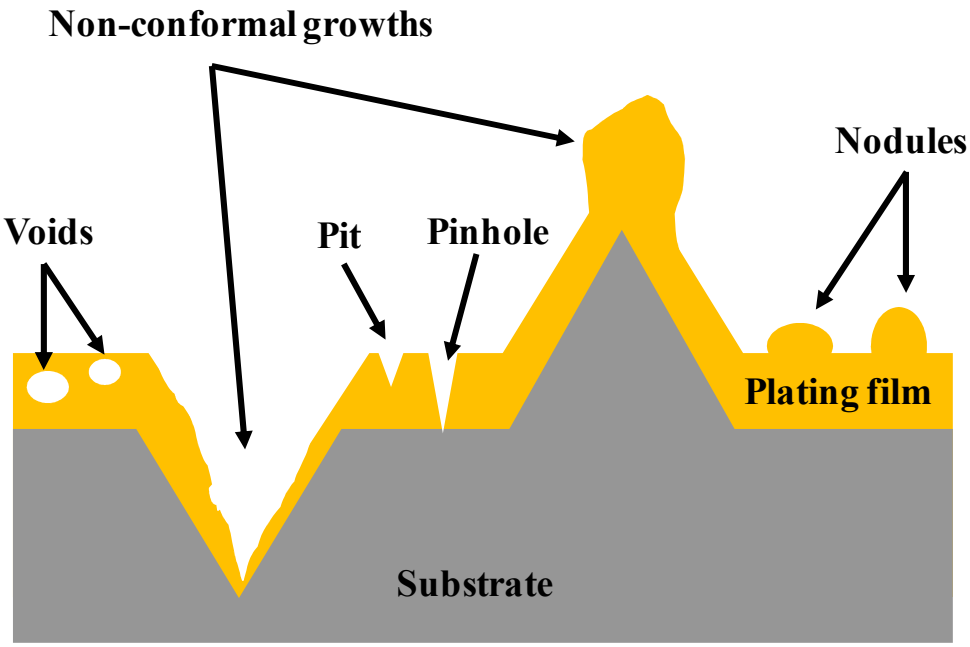

Fig. 1.4 The defects which occurs in film formation.

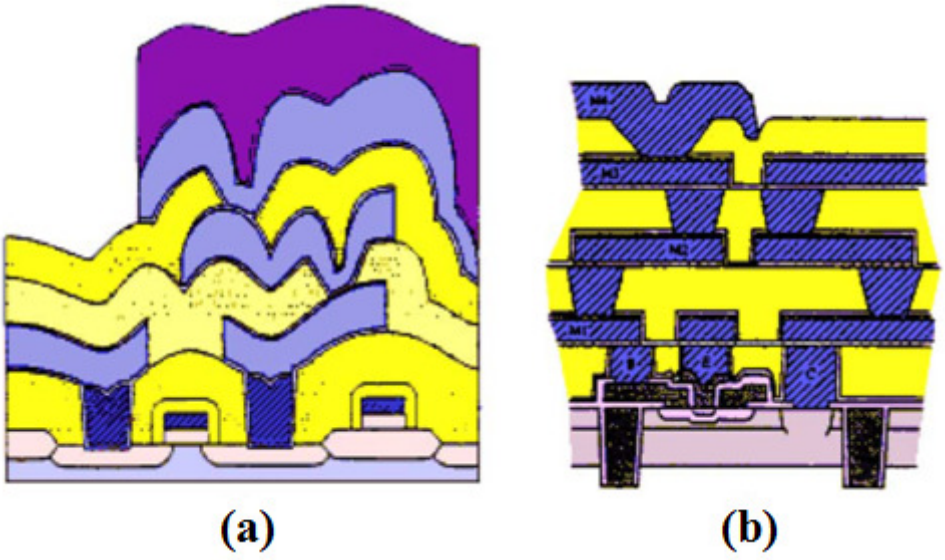

Fig. 1.5 (a) Schematic of a non-planarized and (b) planarized multilayer interconnect.[22]

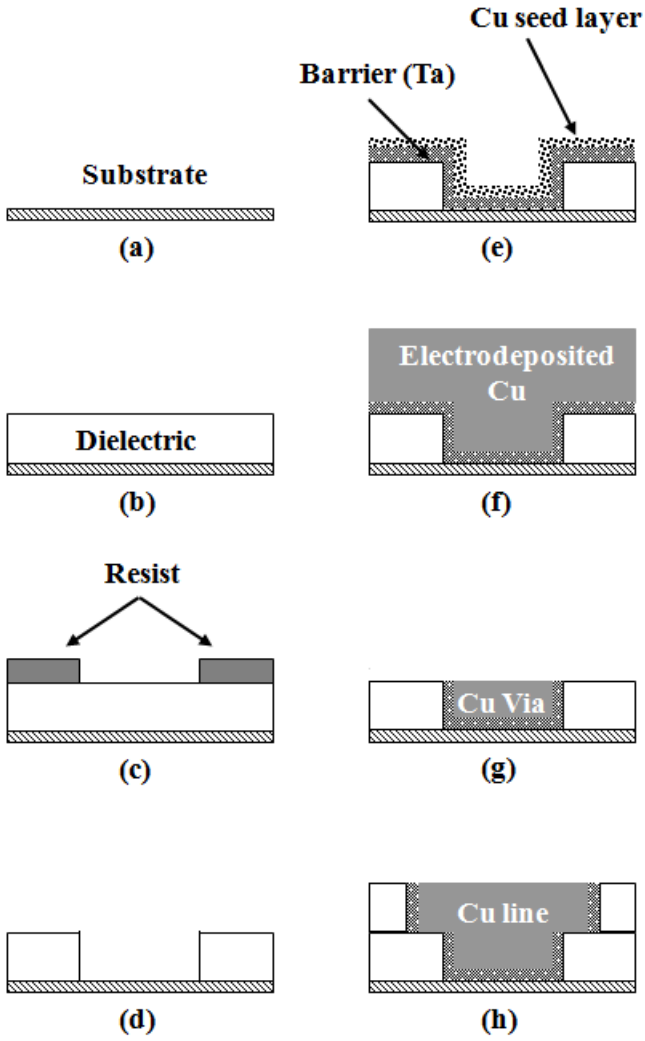

Fig. 1.6 Process steps for forming Cu interconnects using the single damascene process (dielectric patterning): (a) planarized substrate; (b) dielectric deposition; (c) dielectric RIE through photoresist mask; (d) etched insulator; (e) deposition of diffusion barrier (Ta) and Cu seed layer; (f) electrodeposition of Cu into a via (vertical interconnection); (g) CMP of Cu excess; (h) patterning and deposition of Cu line (wire).[12]

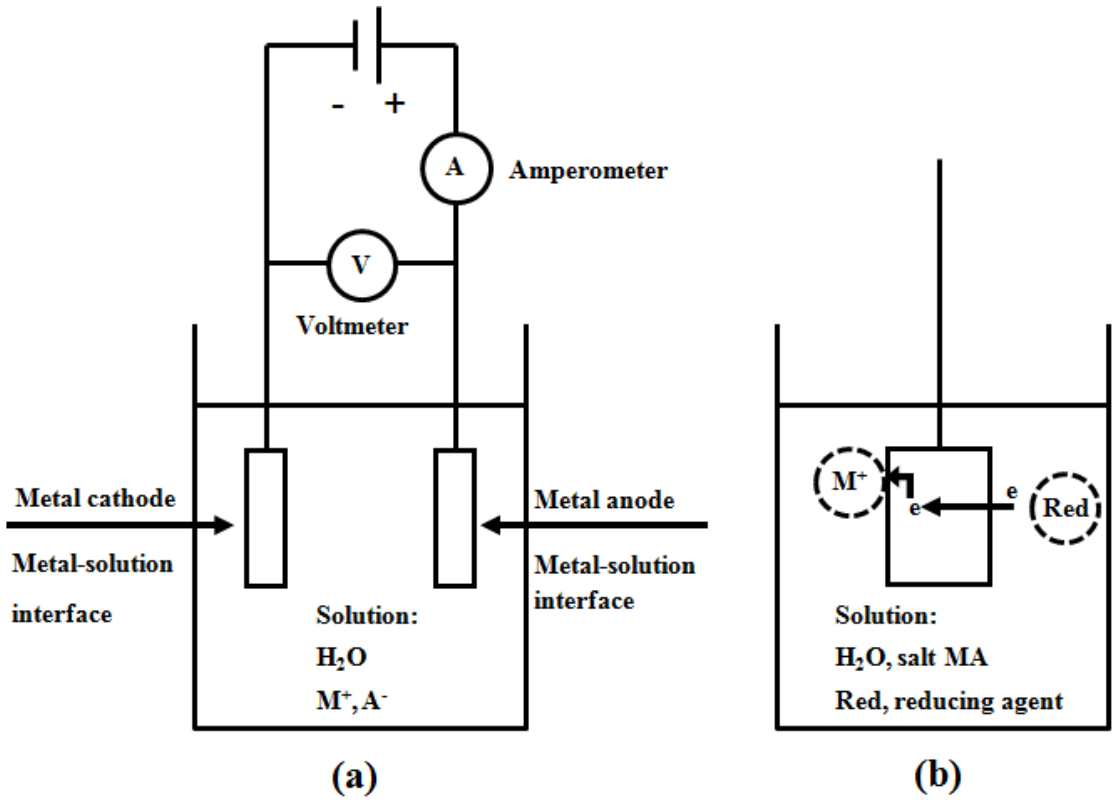

Fig. 1.7 (a) Electrolytic cell for electrodeposition of metal, M, from an aqueous solution of metal salt, MA, (b) Electrolytic cell for electroless deposition of metal, M, from an aqueous solution of metal salt, MA and a reducing agent Red.[9]

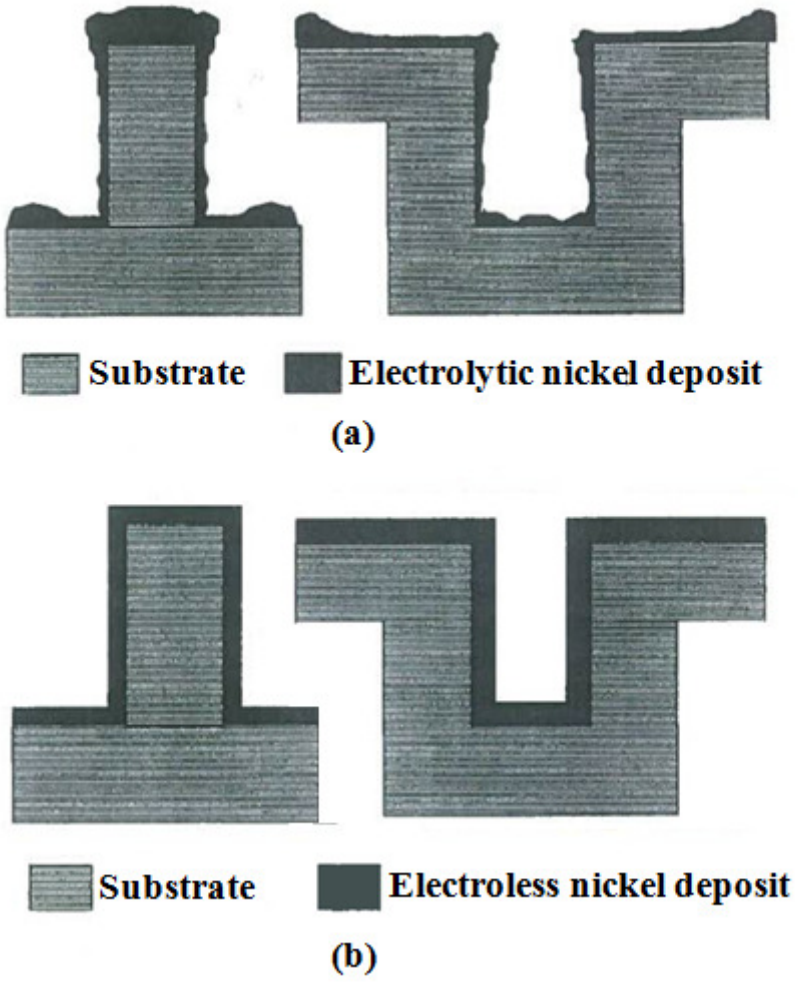

Fig. 1.8 Coverage and thickness uniformity of (a) electroplate nickel and (b) electroless Ni-P deposits on the substrates.[25]

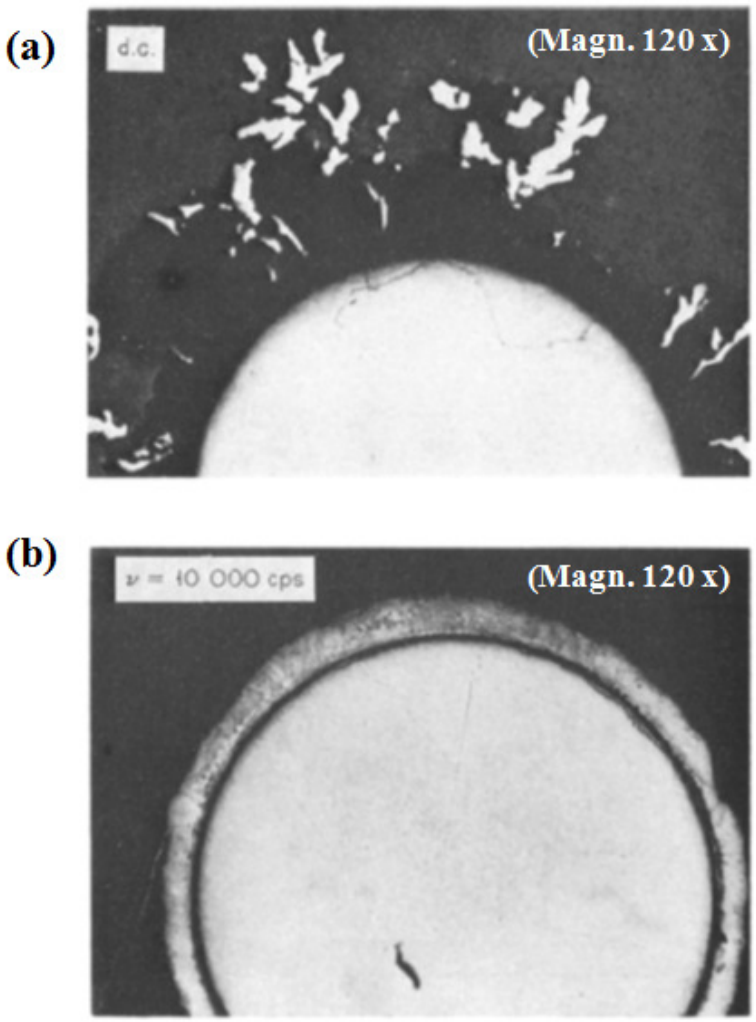

Fig. 1.9 Photomicrographs of zinc deposited onto copper wire by (a) a direct current electroplating and (b) a pulse electroplating.[33]

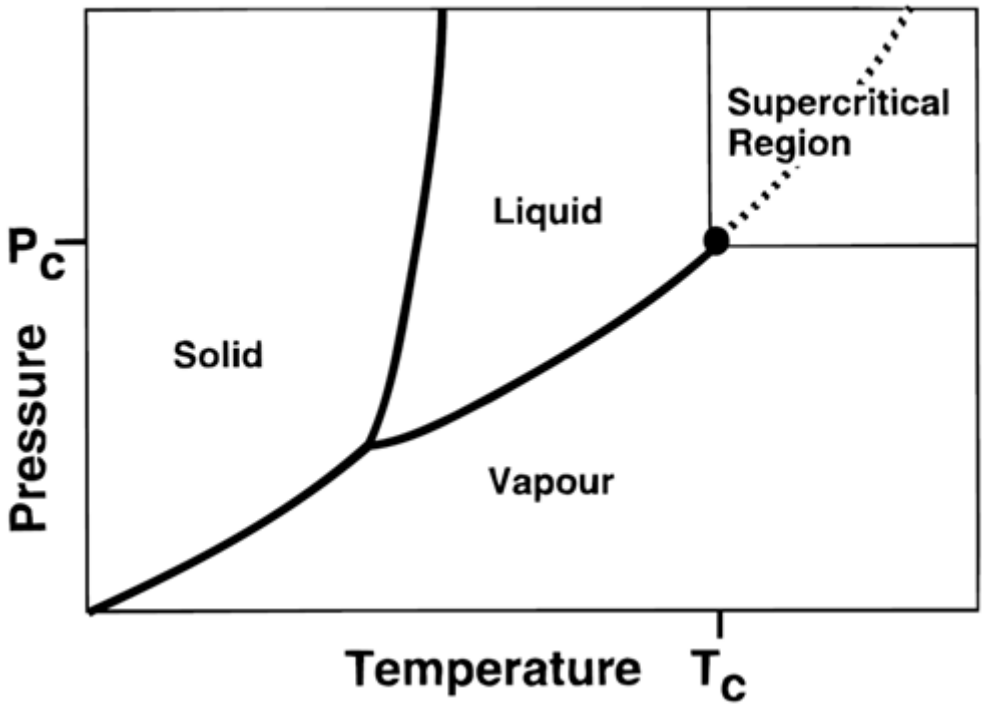

Fig. 1.10 P-T phase diagram for a pure substance, which is traditionally used to define the supercritical region. The dotted line indicates approximately the conditions needed to maintain the critical density at temperatures above Tc.[34]

Parameter	Phase		
	Gases	SCF	Liquids
Density (kg/m^3)	0.6-2.0	300-900	700-1600
Diffusion coeffcient (10^{-9} m^2/s)	1000-4000	20-700	0.2-2.0
Viscosity (10^{-5} Pa·s)	1-3	1-9	200-300
Kinetic viscosity (10^{-7} m^2/s)	100	1-10	10
Thermal conductivity (10^{-3} W/mK)	1	1-100	100

Fig. 1.11 Comparison of selected properties of supercritical fluids (SCF) to those of liquids and gases.[38]

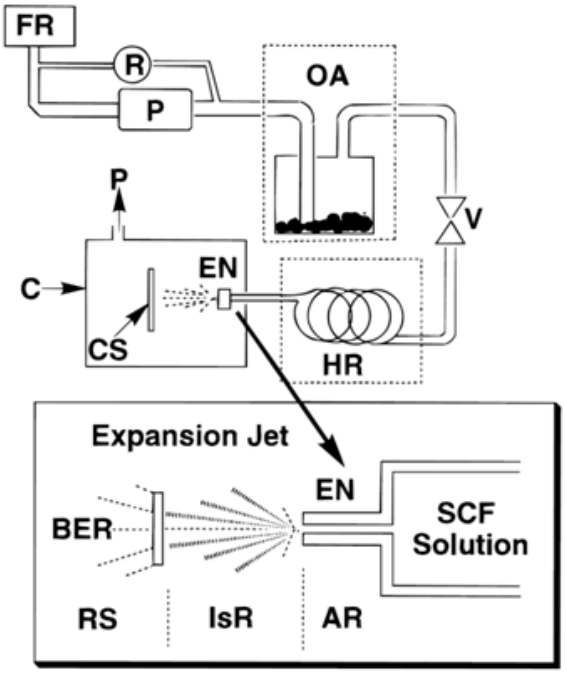

Fig. 1.12 Schematic illustration of the RESS apparatus as used for supercritical water. Inset: the RESS expansion. FR, fluid reservoir; R, pressure regulator; P, pump; OA, optional autoclave; V, valve; HR heated region; EN, expansion nozzle; CS, collection surface; C, collection chamber; AR, adiabatic region; IsR, isentropic region; RS,RESS spray; BER, background expansion region.[34]

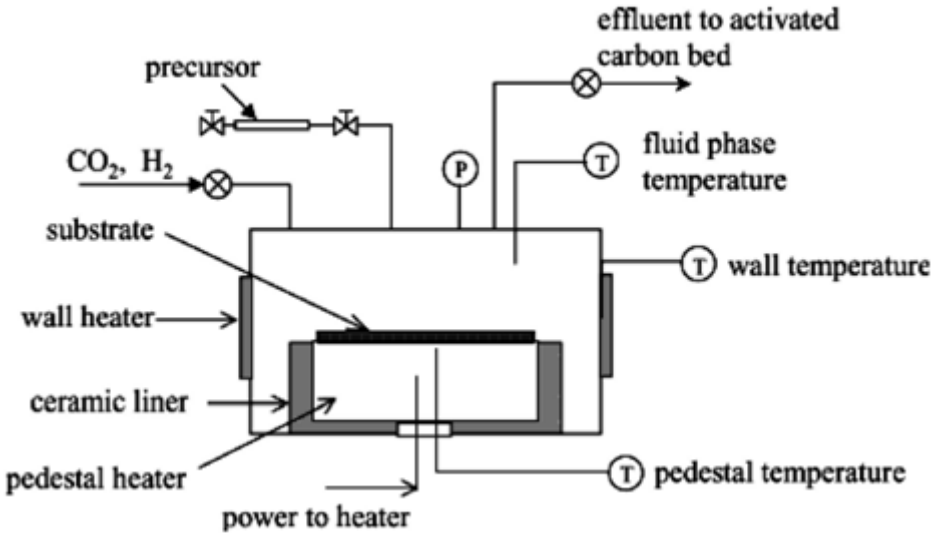

Fig. 1.13 Schematic of the high-pressure cold-wall deposition system.[45]

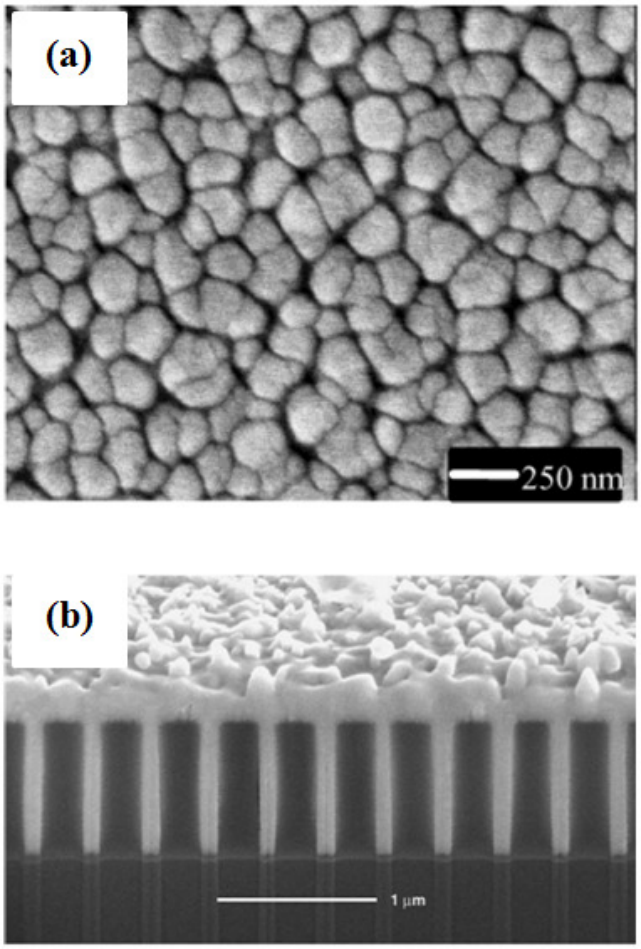

Fig. 1.14 (a) SEM images of Ni films deposited at 448 K and 215 atm from $NiCp_2$ (0.15wt%) in CO_2 solution onto native oxide of Si. (b) a FIB-SEM image of a Ni film deposited at 333 K and 140 atm provides evidence of a narrow seam within the trenches.[46,47]

CHAPTER 2

ELP-SCE – A Novel Electroless Plating Method Using Supercritical CO_2 Emulsion

2.1. Introduction

Electroless plating (ELP) has a low processing temperature, a high metal-ion transportation density, the ability to deposit on electrically nonconductive materials, a more uniform thickness for products of any shape, and a simple deposition mechanism.[1,2] A wet process such as ELP can serve as a superior alternative for a three-dimensional (3D) integration technology. The disadvantages of ELP are the high viscosity of the solution and anomalous growths in the plating film caused by the pretreatment condition. These disadvantages have interfered with the formation of microstructures for electronic devices and MEMS.

The key requirement for forming a uniform, conformal thin film over a complex 3D micro/nanostructure will be to improve the transport properties. To

this end, we propose a technique based on the criteria mentioned above. Specifically, we proposed an ELP method using dense carbon dioxide (CO_2) beyond the critical point as a solvent. The changeable density of dense CO_2 enables excellent control of the intermolecular interactions, and the high density and diffusivity of the material assure that the plating films can form over nanoscale areas with outstanding reliability. Supercritical carbon dioxide (sc–CO_2), however, has been found to be unsuitable as a medium for plating reactions. Metal salts are generally soluble in water, but water and CO_2 tend to mix poorly. The problem can be solved by emulsifying sc–CO_2 and a plating solution, then adding a nonionic surfactant.[3,4] The ELP technique we propose in this study (ELP-SCE) uses a dense CO_2 beyond the critical point. The ELP reaction in ELP-SCE takes place in an emulsion containing dense CO_2. We discuss the surface morphology of the film plated by ELP-SCE, which turns out to have various advantages over the surface morphology of film plated by conventional ELP.

2.2. Experimental method

The ELP methods currently known can be used to deposit 12 different metals (Table 2.1).[2] Decomposition products (phosphorous and boron) in the reducing agent precipitate as the metal deposits, leaving films of the respective alloys. Two or more metals can be deposited at once without much difficulty. ELP methods are used for the deposition of more than 50 alloys of different qualitative compositions, mostly based on nickel, cobalt, and copper. For this study we selected an electroless nickel-phosphorus (Ni-P) plating process. The most widespread type of Ni-P plating uses hypophosphite as the reducing agent.[1,2,5] Three major properties of electroless Ni-P, namely, its hardness, wear resistance, and corrosion resistance, have led to its technical application in many industries, from electronics, automaking, aerospace, and machinery to oil and gas production, power generation, printing, and textiles. The process is generally applied with a stable, acidic Ni-P plating solution, as contact with CO_2 acidifies water due to the formation and dissociation of carbonic acid.

Materials

CO_2 with a minimum purity of 99.99% was purchased from Nippon Tansan Co., Ltd. The experiments were performed with a nonionic surfactant polyoxyethylene lauryl ether ($C_{12}H_{25}(OCH_2CH_2)_{15}OH$) supplied by Toshin Yuka

Kogyo. The electroless Ni–P plating solution had a chemical composition of nickel chloride (9%), sodium hypophosphite (12%), complexing agent (12%), and ion-exchanged water (67%) (Okuno Chemical Industries Co., Ltd.). The substrate was a 99.99% pure film of copper measuring 10×20 mm (Mitsubishi Shindoh Co., Ltd). The substrate was washed with acetone and rinsed in deionized water before each reaction. The grease was removed from the sample by successive dipping in a 10 wt % solution of NaOH and a 10 wt % solution HCl followed by rinsing in deionized water. The sample was added to an activator solution consisting of hydrogen chloride (18%), palladium chloride (0.04%), and ion-exchanged water (81.96%) (Okuno Chemical Industries Co., Ltd.) at 303 K, then rinsed in deionized water. This pretreatment was applied to all copper substrates regardless of the condition of the ELP.

Experimental Apparatus and Method

Fig. 2.1 shows the high-pressure experimental apparatus (Japan Spectra Company) used for the ELP. The temperature variation of each run was confirmed to be less than 1.0 K. The maximum working temperature and the maximum pressure were 424 K and 50 MPa, respectively. The reactor was a stainless steel 316 vessel with an internal volume of 50 mL, kept in a temperature-controlled air bath (Fig. 2.2). A magnetic agitator with a cross-

magnetic stirrer bar was placed within the reactor and the activated substrate was attached to the reactor with stainless wires. A plating reaction within a reactor starts only upon contact between the substrate and plating solution. As such, the substrate position in a reactor affects both the reproducibility and surface morphology of the ELP film. Yan et al. demonstrated the dispersion behaviors of a ternary system composed of dense CO_2, an electroplating (EP) solution, and a surfactant.[6] Their experiment was performed in a high-pressure view cell with an internal volume of 45 mL. In the absence of stirring, two separated phases, namely, a transparent upper CO_2 phase and a clear green lower phase (the nickel EP solution) were observed at 323 K and 10 MPa. The ternary system with the CO_2 volume fraction of 0.2 was stirred at 400 rpm, as shown in Fig. 2.3. The CO_2 dispersed into the plating solution with stirring, and the light scattering from the small CO_2 drops in the solution increased the turbidity of the system. In our experiment, before the ELP reaction, the electroless Ni–P plating solution (30 mL) and surfactant (surfactant concentration: 1.0 wt % to the ELP solution) were placed in the reactor at atmospheric pressure. Next, liquid CO_2 was pumped into the cell by a high performance liquid chromatography (HPLC) pump until a predetermined pressure was reached. The ELP reaction was performed at a temperature of 353 K and a pressure of 15 MPa in a constantly agitating ternary system stirred

at a speed of 500 rpm. The reaction commenced from the start of agitation. In the Results and Discussion of this chapter we describe the properties of the plated film fabricated by ELP-SCE in comparison with those of film fabricated by conventional ELP. The conventional method was performed under the following experimental conditions: 353 K, atmospheric pressure, a plating solution with a chemical composition identical that used in ELP-SCE, constant stirring at a speed of 50 rpm.

Analysis

An optical microscope (Digital Microscope VHX-500, Keyence. Co., Ltd.) and scanning electron microscope (FE-SEM, S-4500, Hitachi High-Technologies Co., Ltd.) were used to study the surfaces of the plated Ni–P films. A surface texture measuring instrument (Surfcom 480A, Tokyo Seimitsu Co., Ltd.) with a diamond-tipped detector (2 μm tip radius) was used to measure the average surface roughness (*Ra*) to a minimum height resolution of 1 nm (height measurement range: 80 μm). The average *Ra* was calculated from measurements at five points or more. The film thickness was measured directly from a cross-sectional scanning electron microscopy (SEM) image of a plated Ni–P film fabricated by a focused ion beam system (FB-2100, Hitachi High-Technologies Co., Ltd.). The phosphorus composition of the fabricated film was

measured by an FE-SEM (S-4300SE, Hitachi High-Technologies Co. Ltd.) equipped for energy-dispersive X-ray spectroscopy (EDX). An accelerating voltage of 20 kV with a collecting time of more than 300 s was applied. X-ray diffraction (XRD) analysis (2θ-ω scans) was performed at room temperature (RT, 298 K) using a PANalytical X'pert Pro Galaxy system equipped with an X'celerator module. The X-ray source was CuKα, and the tube voltage and current were 45 kV and 40 mA, respectively.

2.3. Results and Discussion

2.3.1. Electroless Ni-P Plating in an Emulsion of Supercritical CO_2

Fig. 2.4 shows optical microscope images of a copper substrate and Ni-P films plated over the substrate by ELP-SCE at 15 MPa and 6 MPa. Polishing trace was observable on the copper substrate before pretreatment. The film plated at 15 MPa was uniformly bright and covered both the front and back of the substrate (Fig. 2.4 (b)). The uniform brightness and coverage were attributable to the exact position of the substrate and the uniformity of the emulsion. The formation of emulsion was unstable in the film plated at 6 MPa, beyond the critical point, so the film was thin and even unformed in portions (Fig. 2.4 (c)). The surface roughness (*Ra*) of the plating films was 0.030 μm at 15 MPa and 0.059 μm at 6 MPa.

If CO_2 exceeds a critical point, the density will rise rapidly. While the CO_2 density at 323 K and 6 MPa is only 0.1 kg・L^{-1}, it reaches 0.7 kg・L^{-1} at the higher pressure of 15 MPa.[8] Moreover, Sone et al. reported that in a ternary system of water, surfactant, and CO_2, the CO_2 formation in the water emulsion by the surfactant is affected not only by the temperature and pressure, but also agitation.[4] They also found, in a similar experiment, that no emulsion was

formed below the critical point. With ELP-SCE, a stable emulsion forms when the CO_2 density approaches the liquid phase, and a uniform plating film can be deposited.

According to an as-deposited coating surface composition analysis by EDX, the Ni-P film formed by ELP-SCE was composed of 20 wt % phosphorus. When the phosphorus content increases, the microstructure of an electroless Ni-P deposit changes from a mixture of amorphous and nanocrystalline phases to a fully amorphous phase.[5] The structure of our Ni-P film was confirmed to be amorphous by XRD. Amorphous profiles with a wide angular range of 40-45° (2θ) appear nearby a 2θ position corresponding to the Ni {111} plane. The copper substrate underneath was responsible for the Cu diffraction peaks in the profiles of the Ni-P film formed by ELP-SCE. The peaks appear because the coated-deposit was too thin (1.0 μm less) to totally absorb the penetration of the X-ray beam (Fig. 2.5).

2.3.2. Surface Morphology of Conventional and Novel Electroless Ni-P deposits

We used an optical microscope to observe the surface features of a Ni–P film formed by conventional ELP, another Ni–P film formed by ELP-SCE, and a pure copper substrate (Fig. 2.6). The only clear difference in defects between the two Ni–P films was a polishing trace on the copper substrate. As is widely known, thin films fabricated by ELP have smaller pinholes and cracks than those fabricated by EP.

SEM observations reveal clear differences between the surface morphologies of the Ni–P films and the substrate activated by catalytic Pd, as shown in Fig. 2.7. The thickness of the Ni–P film fabricated by conventional ELP was 0.3 μm, while that fabricated by ELP-SCE was 0.8 μm. Nodules were observed on the Ni–P film fabricated by conventional ELP in the early stage of the reaction, as shown in Fig. 2.7 (b). This nodule formation was the result of concentrated nickel reactions over a localized area. Earlier reports have confirmed that the nickel nucleus appears and grows on the palladium nucleus on the surface of the substrate.[9-11] These nodules become a serious problem when they form in films fabricated by ELP on fine electronic devices and MEMS. Meanwhile, the thin film fabricated by ELP-SCE was free from nodules and pinholes, but its thickness was still more than double that of the thin film

fabricated by conventional ELP. The only particles observed were extremely fine, with diameters of several tens of nm or less (Fig. 2.7 (a)).

Fig. 2.8 shows how variations in the reaction time influence the surface features of the Ni–P films formed by conventional ELP and by ELP-SCE. The plating films formed by conventional plating for 5.0 and 30 min had thicknesses of 0.8 and 4.9 μm, respectively. The plating films formed by ELP-SCE for 360 and 540 min had thicknesses of 0.9 and 1.0 μm, respectively. The SEM images reveal nodules on all of the surfaces of the Ni–P films fabricated by conventional ELP (Fig. 2.7 (b), 2.8 (c), and 2.8 (d)). The images also show that the nodules increased, both in size (from several hundred nm to over several μm) and in number, as the reaction time increased.

Meanwhile, the Ni–P film fabricated by ELP-SCE was free of nodules (Fig. 2.7 (a)) and had an extremely uniform surface (Figs. 2.8 (a) and 2.8 (b)). These results differed considerably from the changes in the surface features of conventional ELP films brought about by adjustments in the reaction time and the processing methods for the substrate activation by Pd.[9-11] We also found that our ELP technique could fabricate superb, highly uniform plated films even when the substrate pretreatment, reaction temperature, and chemical composition of the electroless Ni–P plating solution were all identical to those used in conventional ELP. On this basis, we surmise that our ELP technique

may be effective in suppressing the growth of nodules.

Fig. 2.9 shows the roughness curves on the surfaces of the Ni–P films formed by ELP-SCE, by conventional ELP, and by surface activation of the substrate. The evaluation length of the surface roughness measurement was 1.250 mm. The activated substrate had an *Ra* of 0.040 μm. The conventional ELP had an *Ra* of 0.048 μm and a rougher surface than the activated substrate. Previous reports have shown how activation processing changes the surface morphologies and deposition behaviors of electroless Ni–P films.[9-11] Meanwhile, ELP-SCE formed a film with improved smoothness (*Ra* of 0.030 μm) under the same activation processing conditions used for conventional ELP. We also found that the film thickness conferred a strong influence on the surface roughness. The thin film formed by ELP-SCE was very smooth, though it was still more than twice as thick as the film fabricated by conventional ELP. These results demonstrate that ELP-SCE suppressed the deposition reaction of the locally concentrated nickel. We can also see, in Fig. 2.7 and Fig. 2.8, that no nodules were formed.

The conventional ELP was performed at 353 K and atmospheric pressure. ELP-SCE was performed at 353 K and 15 MPa. Fig. 2.10 shows the relationship between the surface roughness and reaction time. The surface of the Ni–P film fabricated by the conventional ELP roughened as the reaction time increased.

The roughness of the Ni–P film formed by ELP-SCE, meanwhile, showed no dependence on the reaction time. Nodules appeared on the surfaces of the Ni–P films fabricated by conventional ELP at all reaction times, and the nodules grew as the reaction times increased. No nodules were observed on the surfaces of any of the Ni–P films fabricated by ELP-SCE, even at the maximum reaction times. The aforementioned results confirm that the excellent smoothness of ELP-SCE film mitigated the influence of the substrate pretreatment and was independent of the reaction time. Fig. 2.7, meanwhile, shows a suppression of the growth of the nodules generated by conventional ELP.

ELP-SCE produced a thin film with high smoothness and outstanding uniformity. The Ni–P film fabricated by conventional ELP with a reaction time of 5 min had a thickness of 0.8 μm, or about the same thickness as ELP-SCe film fabricated with a reaction time of 180 min. The *Ra* of the ELP-SCE film was 0.03 μm, while that of the conventional ELP film was 0.06 μm.

ELP films are generally smoother than EP films and have fewer defects.[2,5,12] Even with ELP, however, defects such as microscopic nodules, pits, and pinholes are difficult to suppress.[1,13-15] Although suppression of a through-hole like a pinhole need a thick film, more nodules form in a thicker film. Nodules also easily form when the underlayer has projecting parts, foreign objects, and nuclear growth sites. Conventional suppression of nodule method

prepares the smoothness and cleanness of an underlayer, while nonlinear diffusion adds reactive species that interfere with film growth over the projecting parts of a plating film (see Fig. 2.11).[16] Further, the pulse electroplating controls the thickness of a diffusion layer and is available to suppress nodule growth.[17]

ELP-SCE formed very smooth thin films whose thicknesses suppressed both nodules and pinholes without exceeding even 1 μm. The pH, reaction temperature, pretreatment, stirring speed, additive, and reactive species concentration in the plating solution all influence the deposition behavior of the ELP film.[1] Yet in our current work we used the same plating solution, reaction temperature, and pretreatment for both ELP-SCE and conventional ELP.

The Ni–P film plated by ELP-SCE was free of pits and pinholes because the hydrogen bubbles produced by the electrolysis of the water were dissolved in the dispersed sc–CO_2 phase of the emulsion.[18] Moreover, ELP-SCE plates the film under high pressure. High-pressure plating failed to deliver good results because hydrogen bubbles were less buoyant in the high-pressure system than at atmospheric pressure. Hence, the larger bubbles prevent the metal from covering the substrate. This, a characteristic effect of plating techniques that use sc-CO_2 emulsion, suppresses the formation of pits or pinholes via the mechanism shown in Fig. 2.12.

The best feature of ELP-SCE is its ability to suppress nodules and other abnormal growths formed by the plating reaction. The electroless metal deposition occurs by repeated 3D nucleation at catalytic sites on the substrate.[19] In 3D growth of the deposited Ni under a low-nucleation-density condition, the deposited Ni grows and the surface roughness increases. Further, an activation processing technique with Pd catalyst can be used to influence the growth of the Ni–P film.[9-11] In the Ni–P films fabricated by conventional ELP in our current experiments, the activation processing roughened the surface and nodule growth was confirmed. Nodule suppression is only attainable when the abovementioned factors exert their effects at the reaction site of the plating. That is, the growth suppression factor of the plating reaction and the state of the diffusion layer that conveys the film onto the substrate must both be influenced. ELP-SCE differs from the conventional method in three ways: the stirring speed, the addition of the surfactant for emulsion formation, and the decrease of the pH by the CO_2 dissolution in the plating solution. Henceforth, we will also need to consider how the collision phenomenon influences the plating film of the CO_2 phase. We will need to collect more evidence to formulate a detailed mechanism for our process. Even so, our experiments have demonstrated that ELP-SCE produces more outstanding results than conventional ELP, forming thin films with high smoothness and superb uniformity.

Summary

This chapter has proposed ELP-SCE, a hybrid technique combining ELP and supercritical fluid technology. The ELP reactions are carried out in an emulsion of sc-CO_2 and an ELP solution with surfactant. ELP-SCE formed a uniform Ni–P film free from the pinholes that typically form from the hydrogen bubbles produced by the electrolysis of water, and free from the nodules that form from the nuclear growth in the ELP reaction.

References

1. G. O. Mallory and J. B. Hajdu, *Electroless Plating: Fundamentals and Applications*, American Electroplaters and Surface Finishers Society, Orlando, FL (1990).
2. A. A. Tracton, in *Coatings Technology Handbook*, 3nd ed., A. Vakelis, Editor, p. 27-1, CRC Press Taylor & Francis Group, New York (2006).
3. H. Yoshida, M. Sone, A. Mizushima, K. Abe, X. T. Tao, S. Ichihara, and S. Miyata, *Chem. Lett.*, **11**, 1086 (2002).
4. H. Yoshida, M. Sone, H. Wakabayashi, H. Yan, K. Abe, X. T. Tao, A. Mizushiama, S. Ichihara, and S. Miyata, *Surf. Coating. Tech.*, **446**, 194 (2004).
5. W. Sha, X. Wu and K. G. Keong, *Electroless Copper and Nickel-phosphorus Plating: Processing, Characterization and Modeling*, Woodhead Publishing, Cambridge, (2011).
6. H. Yan, M. Sone, A. Mizushima, T. Nagai, K. Abe, S. Ichihara, and S. Miyata, *Surf. Coat. Technol.*, **187**, 86 (2004).
7. JIS-2001, JIS-1994, JIS-1982, ISO-1997, ISO-1984, DIN-1990, ASME-1995.
8. Y. Imai, *Hyomen Gijutsu*, **56**, 74 (2005).
9. H. Watanabe and H. Honma, *J. Electrochem. Soc.*, **144**, 471 (1997).
10. S. Y. Chang, C. J. Hsu, R. H. Fang, and S. J. Lin, *J. Electrochem. Soc.*, **150**,

C603 (2003).

11. T. Tsunoda, H. Nagashima, H. Nishinakayama, H. Watanabe, and H. Honma, *Hyomen Gijutsu*, **56**, 463 (2005).

12. M. Paunovic and M. Schlesinger, *Fundamentals of Electrochemical Deposition*, 2nd ed., John Wiley & Sons, Hoboken, NJ (2006).

13. Y. Nakamaru, T. Joya, K. Tashiro, and H. Honma, *Hyomen Gijutsu*, **60**, 661 (2009).

14. K. Tashiro, S. Yamamoto, Y. Hashimoto, S. Kawashima, and H. Honma, *Hyomen Gijutsu,* **53**, 459 (2002).

15. W. J. Cheong, B. L. Luan, and D. W. Shoesmith, *Appl. Sur. Sci*., **229**, 282 (2004).

16. J. W. M. Jacobs and J. M. G. Rikken, *J. Electrochem. Soc*., **135**, 2822 (1988).

17. M. S. Chandrasekar and M. Pushpavanam, *Electrochim. Acta*, **53**, 3313 (2008).

18. H. Yoshida, M. Sone, H. Wakabayashi, H. Yan, K. Abe, X. T. Tao, A. Mizushima, S. Ichihara, and S. Myata, *Thin Solid Films*, **446**, 194 (2004).

19. H. H. Hsu, J. W. Yeh, and S. J. Lin, *J. Electrochem. Soc*., **150**, C813 (2003).

Table 2.1 Coating Obtained by Electroless Plating

	Reducing Agent						
Metal	**$H_2PO_2^-$**	**N_2H_4**	**CH_2O**	**BH_4^-**	**RBH_3**	**Me ions**	**Others**
Ni	**Ni-P**	**Ni**		**Ni-B**	**Ni-B**		
Co	**Co-P**	**Co**	**Co**	**Co-B**	**Co-B**		
Fe				**Fe-B**			
Cu	**Cu**	**Cu**	**Cu**	**Cu**	**Cu**	**Cu**	
Ag		**Ag**	**Ag**	**Ag**	**Ag**	**Ag**	**Ag**
Au		**Au**	**Au**	**Au**	**Au**		**Au**
Pd	**Pd-P**	**Pd**	**Pd**	**Pd-B**	**Pd-B**		
Rh		**Rh**					**Rh**
Ru				**Ru**			
Pt		**Pt**		**Pt**			**Pt**
Sn						**Sn**	
Pb			**Pb**				

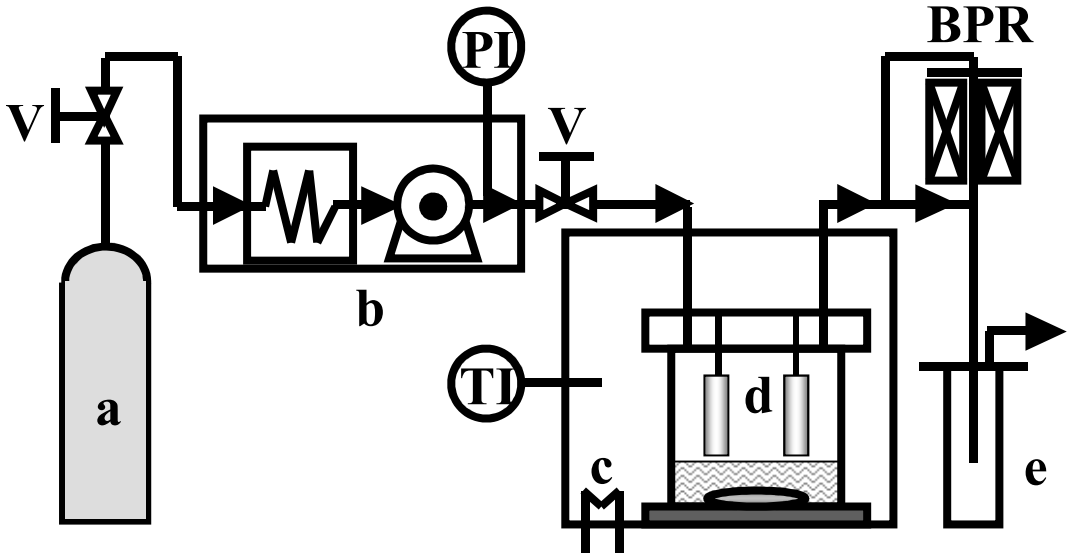

Fig. 2.1 Experimental apparatus used for batch reaction in our electroless plating experiments beyond the critical point of CO_2; (a) CO_2 cylinder; (b) cooler and high pressure pump; (c) temperature controlled air bath; (d) reactor with magnetic stirrer; and (e) trap; BPR: back-pressure regulator; PI: pressure indicator; TI: temperature indicator; V: valves.

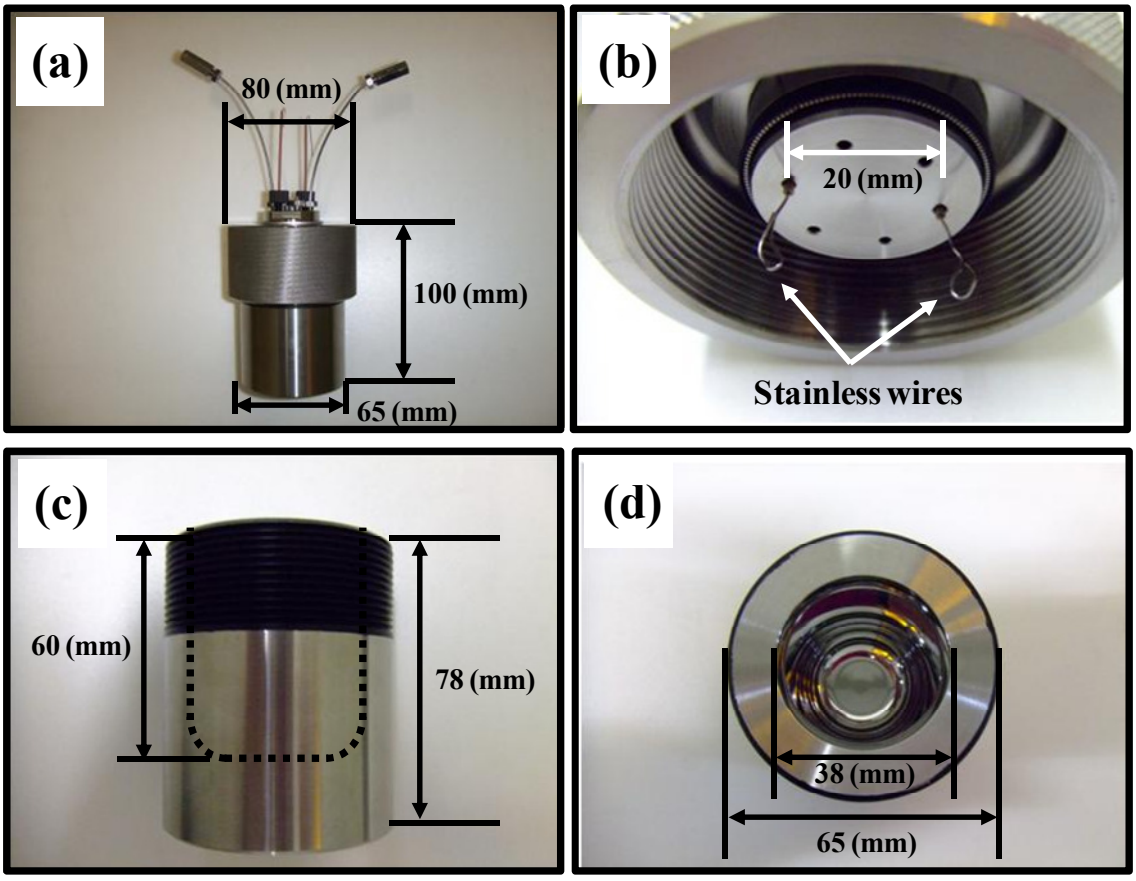

Fig. 2.2 High pressure reactor; (a) external view; (b) lid; (c) outer size of reactor; (d) inside size of reactor.

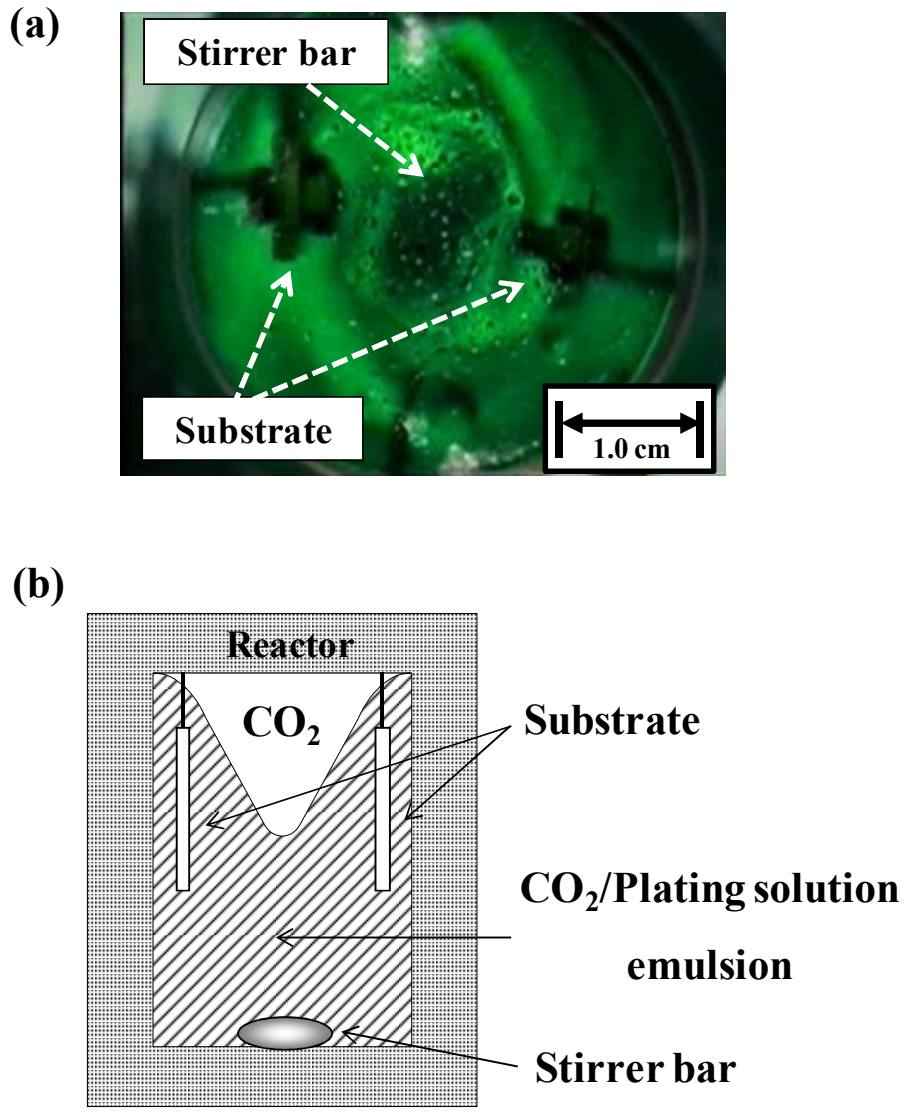

Fig. 2.3 (a) Photographs of the dispersion behavior of system containing supercritical CO_2 electroplating solution with surfactant at 323 K, 10MPa, and agitation speed is 400rpm, (b) schematic representation of the state in the reactor under agitating.[6]

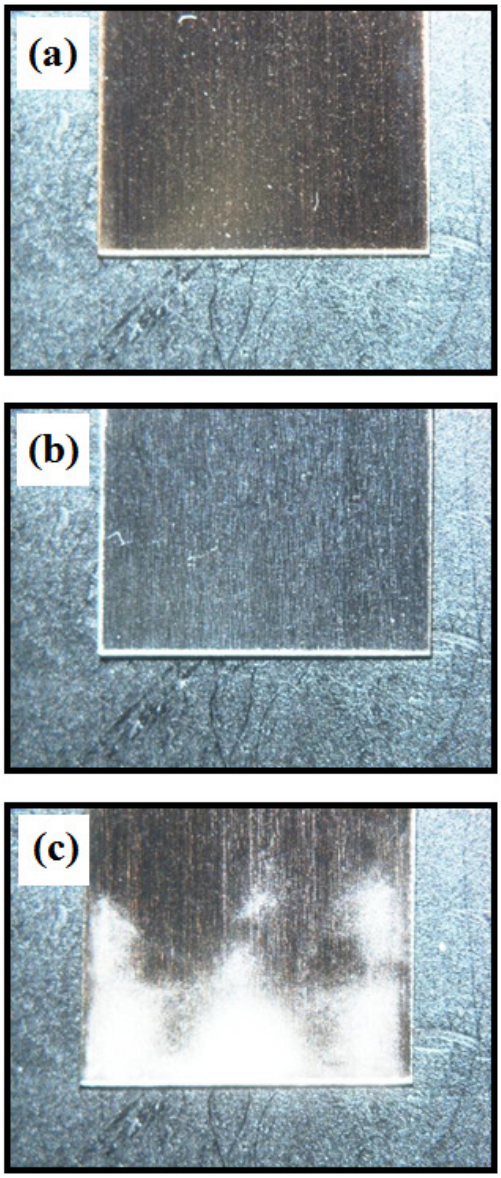

Fig. 2.4 Optical microscopy images of (a) pure copper substrate and Ni–P films plated from novel electroless plating at 353 K for 60 min (b) at 15 MPa and (c) at 6 MPa.

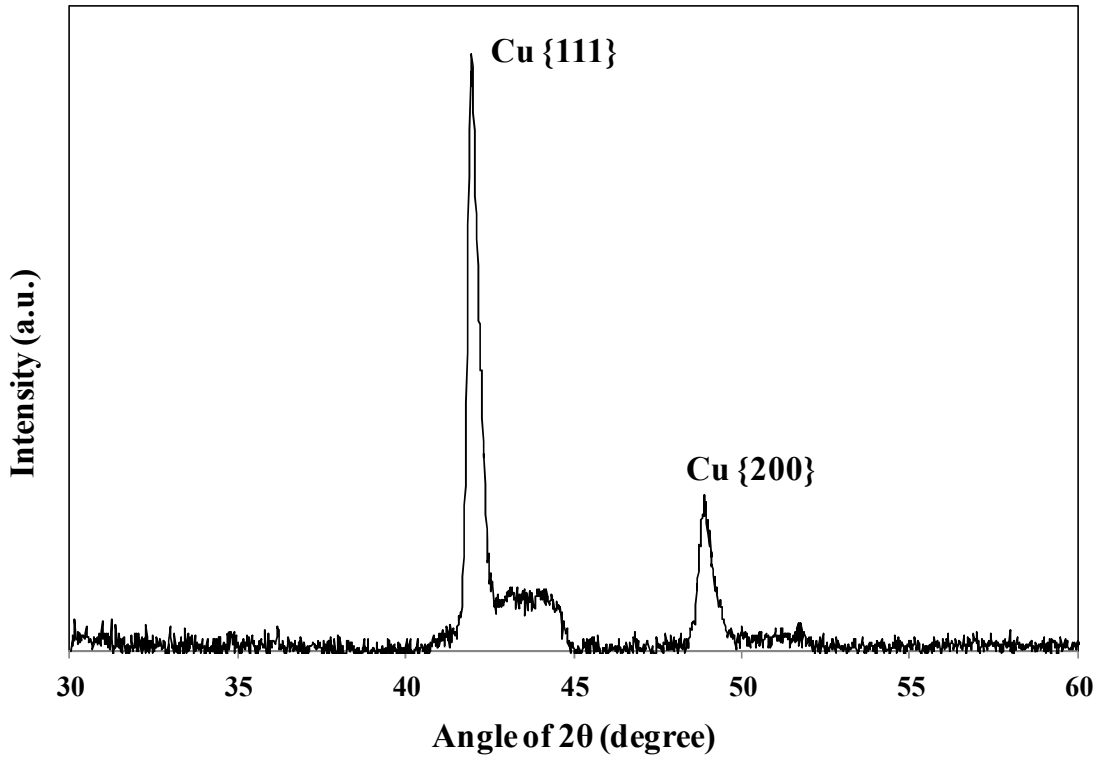

Fig. 2.5 XRD spectrum of Ni-P film plated from our electroless plating at 353K and 15 MPa for 180 min.

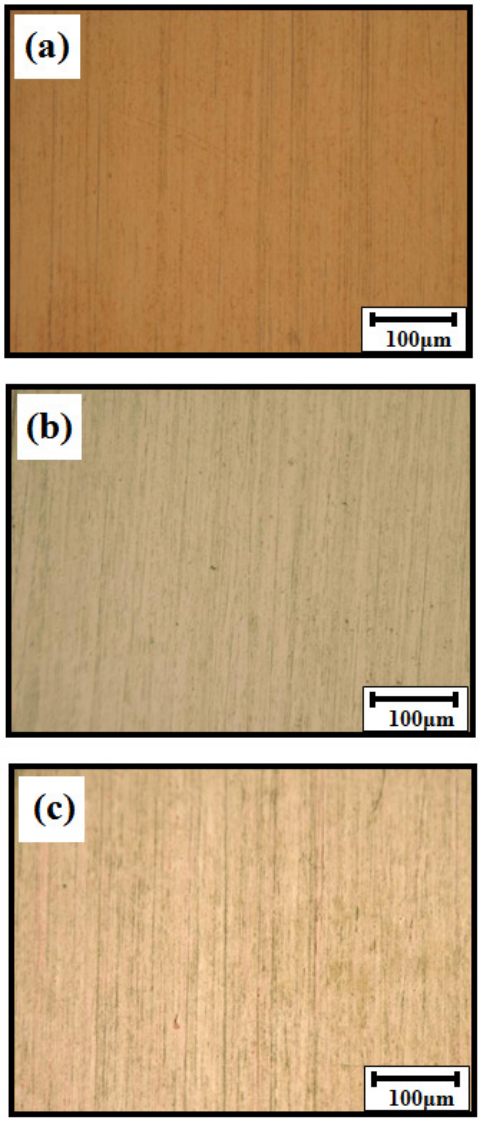

Fig. 2.6 Optical microscopy images of Ni–P films plated from (a) our electroless plating at 353 K and 15 MPa for 180 min (with a film thickness of 0.8 μm), (b) conventional electroless plating at 353 K and atmospheric pressure for 2 min (with a film thickness of 0.3 μm), and (c) pure copper substrate.

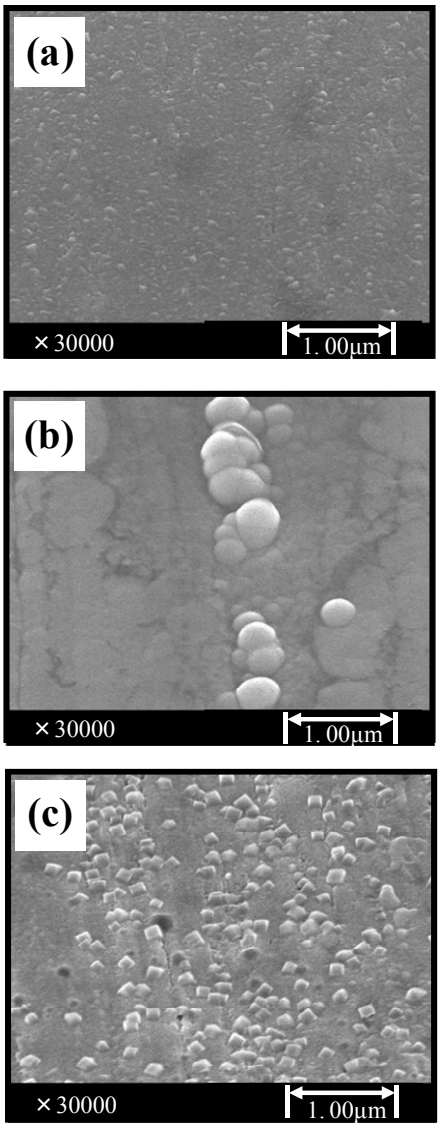

Fig. 2.7 SEM images of Ni–P films plated from (a) novel electroless plating at 353 K and 15 MPa for 180 min (with a film thickness of 0.8 μm), (b) conventional electroless plating at 353 K and atmospheric pressure for 2 min (with a film thickness of 0.3μm), and (c) substrate activated by catalytic Pd.

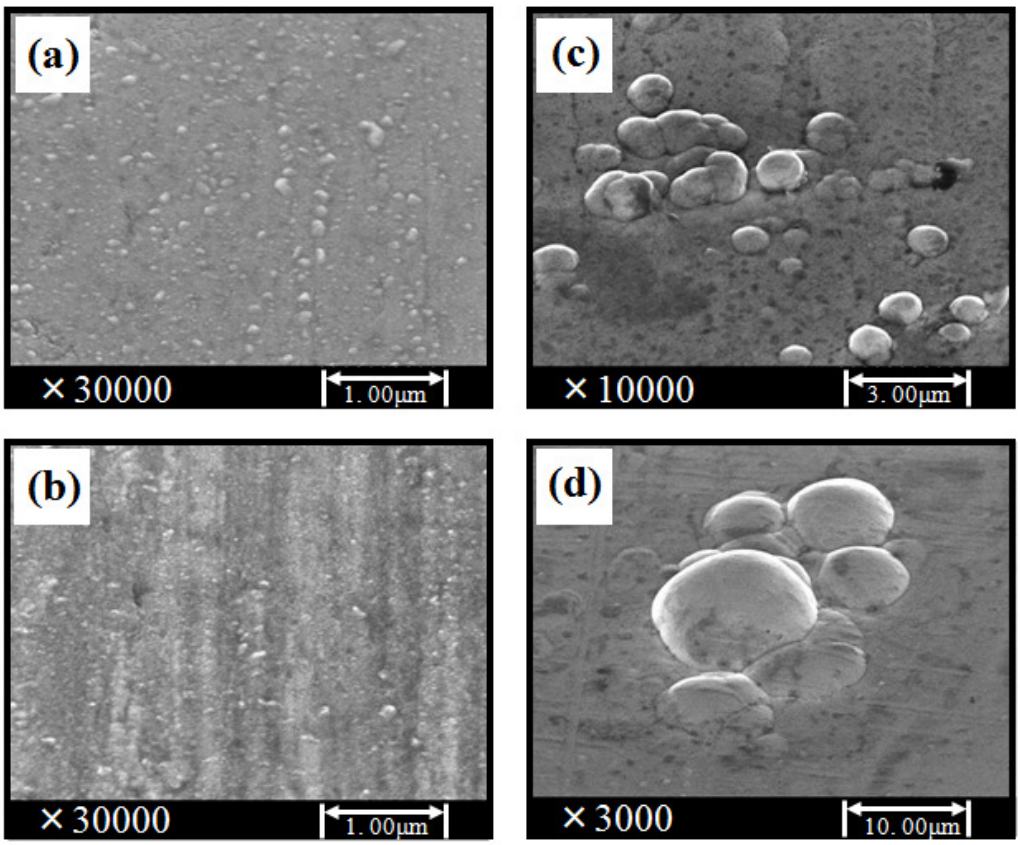

Fig. 2.8 SEM images of Ni–P films plated from our electroless plating at 353 K and 15 MPa for reaction times of (a) 360 min and (b) 540 min, and conventional electroless plating at 353 K and atmospheric pressure for reaction times of (c) 5 min and (d) 30 min.

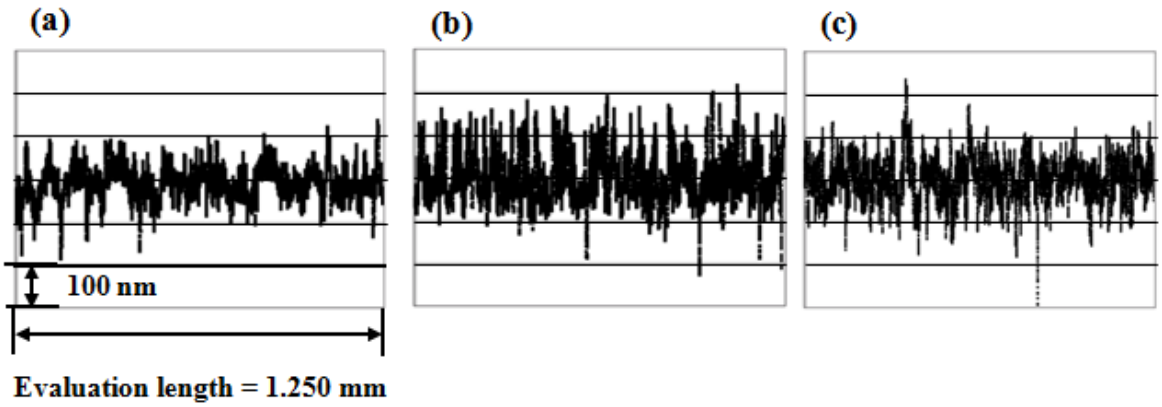

Fig. 2.9 Roughness curves of the surfaces of Ni–P films plated by (a) electroless plating at 353 K and 15 MPa for 180 min (with a film thickness of 0.8 μm), (b) conventional electroless plating at 353 K and atmospheric pressure for 2 min (with a film thickness of 0.3 μm), and (c) substrate activated by catalytic Pd.

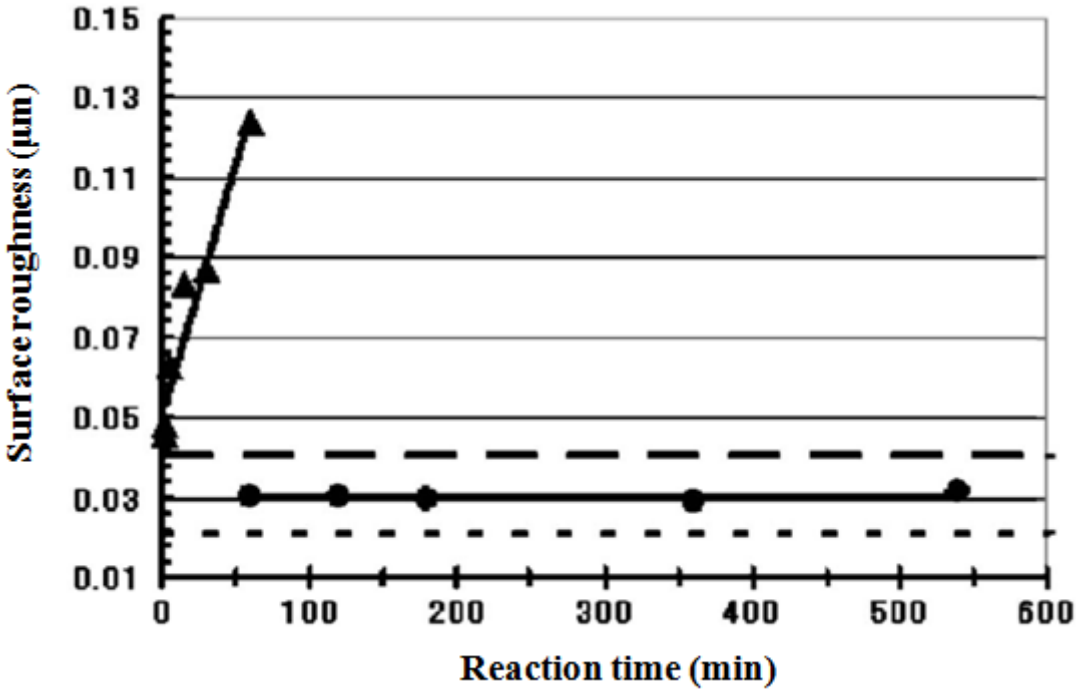

Fig. 2.10 Relationship between surface roughness and reaction time. The surface roughness values of the Ni–P film made by our electroless plating technique are plotted as circles. The linearly approximated curve is shown as a line. The roughness values of the Ni–P film made by conventional electroless plating are plotted as triangles and the linear approximation curve is shown as a line. The dotted line shows the surface roughness of the activated substrate and the fine dotted line shows the surface roughness of the pure copper substrate.

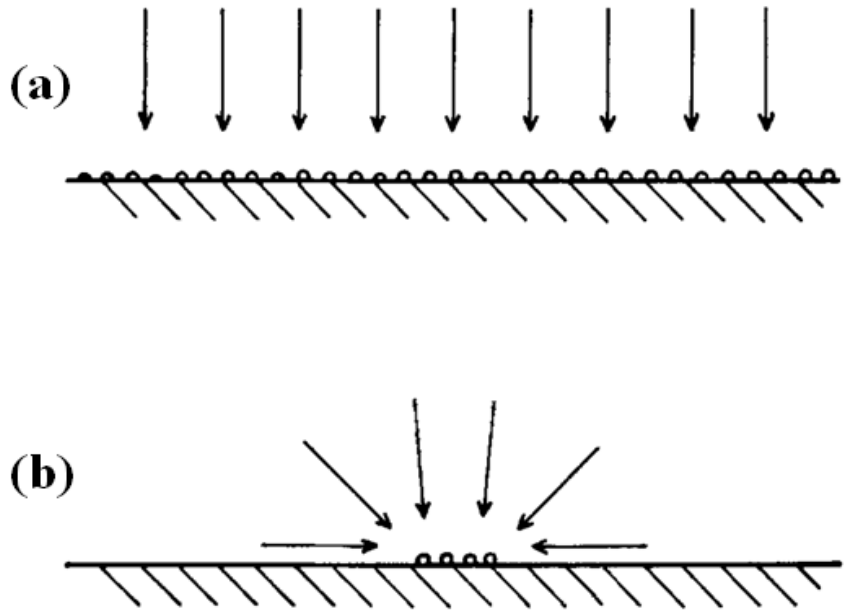

Fig. 2.11 (a) Linear O_2 diffusion to a large activated area. (b) Linear and nonlinear O_2 diffusion to a small pattern of nuclei.[15]

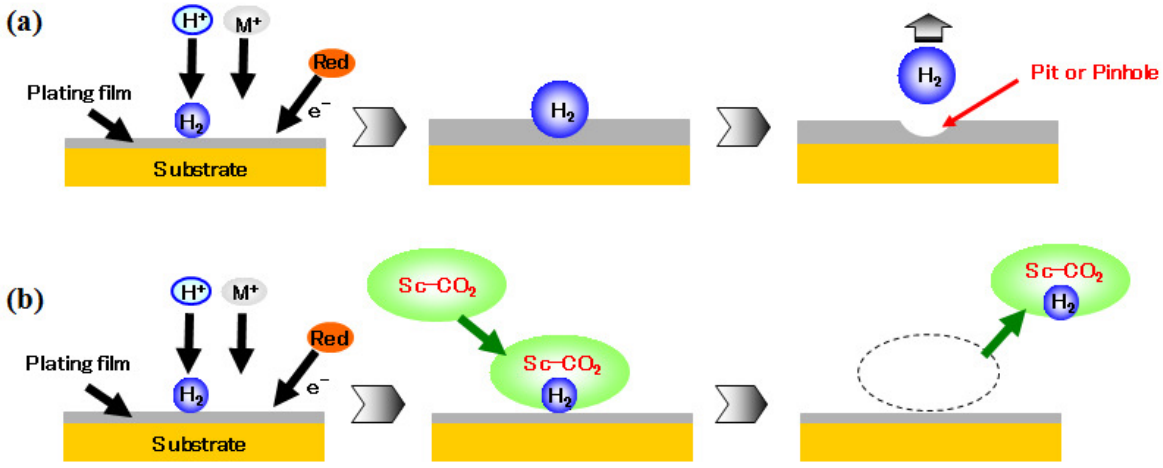

Fig. 2.12 (a) Pinhole formation in conventional electroless plating. (b) Suppressed pinhole formation in novel electroless plating method using supercritical CO_2 emulsion. M: metal, Red: reducing agent, and sc-CO_2: supercritical carbon dioxide.

CHAPTER 3

Reaction Mechanism of Electroless Ni-P Plating in an Emulsion of Supercritical CO_2

3. 1. Introduction

In the last chapter we reported ELP-SCE, a technique for electroless plating using a supercritical carbon dioxide emulsion. Supercritical carbon dioxide (sc-CO_2) has a high and adjustable density and a high diffusivity. These properties of sc-CO_2 are very advantageous for intermolecular interaction control, as they allow the emulsion to move and deposit materials at a nanoscale level of precision. The various merits of the electroless plating (ELP) have attracted considerable attention. These include, most notably, its lower tool cost, low processing temperature, high metal-ion transportation density, good step-coverage capability, and ability to deposit a metal film on a nonconductive specimen after sensitization and activation treatments.[1-5] ELP has two notable disadvantages, namely, the highly viscous solution and anomalous growths in

plating films, such as nodules, pinholes, and voids. ELP-SCE surmounts both of these disadvantages. The Ni–P films obtained by ELP-SCE are extremely uniform and conformal, and completely free from pinholes and nodules. In the last chapter we confirmed the various innovative characteristics of ELP-SCE. The reaction mechanism itself, however, has yet to be sufficiently explained. The further development of the method hinges on a closer understanding of the reaction mechanism and how this mechanism influences the various other factors in the system.

In this part of our study we seek to clarify how the electrochemical reaction of ELP-SCE influences the nodule suppression. Specifically, we discuss the effects of the agitation speed, the surfactant additive, the dissolved oxygen (DO) concentration, and pH in the plating solution.

3.2. Experimental method

Materials

The experiments were performed using carbon dioxide (CO_2) (minimum purity of 99.99%) purchased from Nippon Tansan Co., Ltd. and poly(oxyethylene) lauryl ether [$C_{12}H_{25}(OCH_2CH_2)_{15}OH$], a nonionic surfactant supplied by Toshin Yuka Kogyo. The electroless Ni–P plating solution had a chemical composition of nickel chloride (9%), sodium hypophosphite (12%), complexing agent (12%), and ion-exchanged water (67%) (Okuno Chemical Industries Co., Ltd.). The substrate was a film of 99.99% pure copper measuring 10×20 mm (Mitsubishi Shindoh Co., Ltd.). Each reaction was preceded by a substrate pretreatment consisting of the following steps: a wash in acetone and rinse in deionized water; grease removal by successive dipping in 10 wt % solutions of NaOH and HCl followed by a rinse in deionized water; immersion of the sample in an activator solution of hydrogen chloride (18%), palladium chloride (0.04%), and ion-exchanged water (81.96%) (Okuno Chemical Industries Co., Ltd.) at 303 K; and a final rinse in deionized water. This pretreatment was applied to all copper substrates used in all ELP reactions.

Experimental Apparatus and Method

Fig. 3.1 shows the high-pressure experimental apparatus (Japan Spectra Company). The temperature variation of each run was confirmed to be less than 1.0 K. The maximum working temperature and maximum pressure were 424 K and 50 MPa, respectively. The reaction chamber was a stainless steel 316 vessel with an internal volume of 50 ml, kept in a temperature-controlled air bath. A stainless steel wire was fed through one of several holes in the chamber cap to connect and hang the Cu substrate. A magnetic agitator with a cross-magnetic stirrer bar was placed within the reaction chamber, and the substrate was attached to the reactor with stainless steel wires. Before the ELP reaction, the electroless Ni–P plating solution (30 mL) and surfactant (concentration: 1.0 wt % to the ELP solution) were placed in the reactor at atmospheric pressure. Next, liquid CO_2 was pumped into the cell by a high performance liquid chromatography (HPLC) pump until a predetermined pressure was reached. The Ni-P thin film was electrolessly plated in the emulsion of CO_2 in the Ni-P electroless solution at 353 K and 15 MPa. The properties of the plating film fabricated by ELP-SCE were compared with those of the film fabricated by ELP in the solution alone at different acidities. The ELP with the Ni–P electroless plating solution alone was performed at 353 K under atmospheric pressure with a plating solution of the same chemical composition as that used for ELP-SCE.

The solution was kept in a glass beaker in a temperature-controlled water bath agitated with a magnetic agitator and a cross-magnetic stirrer bar. The substrate was attached to the beaker by stainless steel wires.

Analysis

An optical microscope (digital microscope VHX-1000, Keyence Co., Ltd.) and a field-emission-scanning electron microscope (FE-SEM, S-4500, Hitachi High-Technologies Co., Ltd.) were used to study the surfaces of the plated Ni–P films. A surface texture measuring instrument (Surfcom 480A, Tokyo Seimitsu Co., Ltd.) with a diamond-tipped detector (2 μm tip radius) was used to measure the average surface roughness (*Ra*) to a minimum height resolution of 1 nm (height measurement range: 80 μm). The average *Ra* was calculated from measurements at five points or more. The film thickness was measured directly from a cross-sectional scanning electron microscopy (SEM) image of a plated Ni–P film fabricated by a focused ion beam system (FB-2100, Hitachi High-Technologies Co., Ltd.). The phosphorus composition of the fabricated film was measured by an FE-SEM (S-4300SE, Hitachi High-Technologies Co. Ltd.) equipped for energy-dispersive X-ray spectroscopy (EDX). An accelerating voltage of 20 kV with a collecting time of more than 300 s was applied. The film thickness and phosphorus composition of the fabricated film are shown in

Table 3.1. The DO concentration in the plating bath was measured under the plating condition with a DO meter (UC-12 type, Central Science Co., Ltd., resolution 0.1 mg/L).

3.3. Results and discussion

In discussing the differences between ELP-SCE and the conventional method, we refer to the results of the experiments performed using the basic plating conditions of the conventional method described in the previous chapter: atmospheric pressure, reaction time of 5 min, 353 K, stirring speed of 50 rpm. Many nodules were observed in the first sample (sample 1) fabricated under these conditions (Fig. 3.2). Table 3.2 shows the plating conditions of the sample used to confirm the influence on nodule suppression.

3.3.1. Effect of Agitation.

The electrodeposited films and electrochemical kinetics parameters were affected by the agitation.[6,7] Two factors were found to substantially compromise the plating uniformity; namely, bubble formation on the active sites induced by hydrogen evolution during the plating, and the retention of the bubbles on the film surface. Agitation to allow the flow of solution across the substrate prevents the bubble retention at the plating surface and improves the plating uniformity. The agitation speed in ELP-SCE was 500 rpm. We confirmed the influence of the agitation speed on the surface morphology by fabricating a plating film by the conventional method with agitation set at the same speed, 500 rpm. This film (sample 2) had a surface roughness of Ra = 0.032 μm, as

measured by a surface texture measuring instrument, and on macroscopic inspection its flatness was superior to that of the plating film by the conventional method with no change in agitation speed (sample 1). Under SEM observation, however, nodule formation was not suppressed and undulation was observed (Fig. 3.3). Thus, the change of agitation speed alone in the conventional method was ineffective in improving the smoothness of minute areas to a degree comparable to ELP-SCE. The conditions of the ELP-SCE, on the other hand, were expected to reduce the viscosity of the plating reaction field, as the sc–CO_2 component in the emulsion had a viscosity of 30.1 μPa·s at 323 K and 10 MPa.[8] This effect mitigated the influence of the agitation on the surface morphology, the effect seen in the conventional method.

3.3.2. *Effect of Surfactant.*

The surfactant used as a smoothing agent influenced the deposition behavior of the plated film.[1,9,10] For ELP-SCE we added a nonionic surfactant to make the emulsion. Then, for our conventional ELP experiments, we added a nonionic surfactant to the plating solution at a rate similar to that applied for ELP-SCE (surfactant concentration: 1.0 wt % to the ELP solution) and fabricated sample 3 (Fig. 3.4). This method provided a better smoothness than the conventional ELP without surfactant. Furthermore, we obtained a surface

roughness close to that of the film fabricated by ELP-SCE. Nodules, however, were observed on the film fabricated by the conventional electroless plating with the addition of surfactant.

3.3.3. *Effect of Dissolved Oxygen.*

The DO concentration of the plating solution is well known to affect the deposition behavior on a small substrate area.[6] The DO effect has been explained with a mixed potential theory. The DO in the plating solution concentrates over small areas of the substrate by nonlinear diffusion.[11] The DO concentration below the ppm level in the plating solution at atmospheric pressure is thus reduced preferentially, which suppresses the metal deposition reaction. The ELP-SCE reaction, on the other hand, is carried out in an emulsion of sc–CO_2 and an electroless plating solution with nonionic surfactants. Agitation by stirring disperses the CO_2 into the plating solution.[12] In our experiments, the agitation of this reaction field at high speed conferred a transport property superior to that observed in conventional ELP, and the volume of high-pressure CO_2 exceeded the volume of DO in the plating solution at the ppm level (reactor containing 20 mL of CO_2). This meant that ELP-SCE conferred the same effect as the DO removal by nitrogen gas bubbling.[13-16] Thus, the DO was removed in the dispersed sc–CO_2 phase of the emulsion and the

influence of the DO was accordingly reduced. The accuracy with which the DO can be measured is influenced when a mixed-solution containing a chloride-like plating liquid is used, and the measurement is also difficult in the plating reaction in ELP-SCE. For the calculation of the DO saturation under each plating condition, the amount of DO of the Ni-P plating solution with nonionic surfactant added and air bubbling for 1 hour was assumed to be 100% (Table 3.3). The DO saturation was 83% under condition 1 and 68% under condition 2. The plating conditions of ELP-SCE decreased the amount of DO in the plating solution. Meanwhile, nodule formation was not suppressed in the plating film fabricated by conventional ELP, the method with a nonionic surfactant added and with a greater amount of DO compared to ELP-SCE (Fig. 3.4). Meanwhile, ELP-SCE, which had less DO than the conventional method, suppressed nodule formation. Thus, our experiments determined that DO was not responsible for suppressing nodule formation in ELP-SCE.

3.3.4. *Effect of pH.*

The reaction mechanism of electroless deposition has been extensively studied.[17] Four principal mechanisms have been proposed to account for the reduction with hypophosphite in alkaline and acid media. Each has been supported. From among these four, our group studied the mechanism by which ELP-SCE suppresses defects on the ELP film. This mechanism is based on the electrochemical processes at work in electroless Ni–P deposition, as expressed in the following equations

$$H_2PO_2^- + H_2O \Rightarrow H_2PO_3^- + 2H^+ + 2e^- \quad (1)$$

$$Ni_2^+ + 2e^- \Rightarrow Ni\downarrow \quad (2)$$

$$2H^+ + 2e^- \Rightarrow H_2\uparrow \quad (3)$$

$$H_2PO_2^- + 2H^+ + e^- \Rightarrow P\downarrow + 2H_2O \quad (4)$$

The autocatalytic deposition is a mixed process that results from anodic reactions (oxidation of hypophosphite) and cathodic processes (reduction of the metallic species, hypophosphite, and protons). The electrons required for the reduction of the metal ions are supplied by the reducing agent. Mixed potential theory interprets many electrochemical processes in terms of the electromechanical parameters of the partial electrode reactions.[1] At steady state

equilibrium potential (mixed potential), the rate of deposition ($i_{deposition}$) is equal to both the rate of the oxidation of hypophosphite (anodic current, i_{Red}) and the rate of the cathodic reactions (cathodic current, $i_{Ni} + i_H + i_P$). That is:

$$i_{deposition} = i_{Red} = i_{Ni} + i_H + i_P \tag{5}$$

Here, we focused on the reaction of the hydrogen gas generation, the process expressed by equation (3). In ELP-SCE, the sc-CO_2 phase diffuses and dissolves in the plating solution and the pH of the plating solution decreases in the manner shown in equation (6)[18]

$$CO_2 + H_2O \Leftrightarrow H_2CO_3 \Leftrightarrow H^+ + HCO_3^- \tag{6}$$

The pH of an emulsion with sc-CO_2, however, is difficult to measure. As a workaround, we adjusted the pH of the plating solution in the ELP method, compared the characteristics of the film fabricated by ELP-SCE with that fabricated by ELP in the solution alone, and verified the pH during the ELP-SCE reaction. HCl solution (10 wt %) was added to the original plating solution (pH 5.3) to adjust the pH to 4.0, then the film was fabricated by ELP in the solution alone. Fig. 3.2, Fig. 3.5, and Table 3.2 show the surface morphologies

and film characteristics of plating films fabricated under different conditions. Clusters of nodules were densely distributed on the surface of the plating film fabricated in the original plating solution. In sample 4, the film fabricated in the ELP solution at pH 4.0 (Fig. 3.5 (a)), however, the growth rate was slow and the nodules were decreased in both size and number. The growth rate of a plating film generally decreases as the pH of the plating solution decreases.[1,19] Here, we adjusted the reaction time of the pH 4.0 plating solution to 20 min, that is, the time required to fabricate a fifth sample (sample 5) with the same thickness as the pH 5.3 plating film, and compared the surface morphologies (Fig. 3.5 (b)). The *Ra* value of sample 5 was close to that of the film fabricated by ELP-SCE, indicating that the nodules were greatly decreased in both size and number compared with the nodules shown in Fig. 3.2. This meant that the H^+ concentration influenced both the smoothing of the plating film and the control of nodule formation.

EDX analysis revealed a far higher phosphorus content in the film fabricated by ELP-SCE than in the film fabricated by ELP in the solution alone (Table 3.1). This finding supports the notion that ELP-SCE increases the H^+ concentration in the plating solution. Yet in the reaction at atmospheric pressure at the temperature of 345 K, we also noted a decrease in the pH of the plating solution from 5.3 before the plating reaction to 5.2 after the reaction. We know

that the pH after the reaction at atmospheric pressure (pH 5.2) can differ from that after the reaction in high-pressure emulsion with CO_2, given that the plating film fabricated by ELP-SCE had a higher phosphorus content than the Ni–P film fabricated in the ELP solution at pH 4.0. While the P concentration of the plating film is conventionally controlled by the pH and reducing agent concentration of the plating solution, both parameters still influence the stability of the plating solution and surface morphology of the plating film. There is evidence to suggest, however, that ELP-SCE can control the P concentration without relying on those methods.[2,20] Drawing from the evidence in previous papers, we can determine, based on the phosphorus value and growth rate of the plating film in the present paper, that the pH of the emulsion with CO_2 can be as low as 4, or even lower, and can never exceed about 4.[1,19] The plating reaction field in ELP-SCE may be in the pH range calculated in the E-pH diagram by Ohno and Haruyama, where H^+ is reduced more easily than the Ni ion.[21] A higher H^+ concentration comes hand in hand with an increased generation of hydrogen gas, which produces a condition that inevitably permits the formation of more pinhole and voids. In our experiments, pinholes were evident in Fig. 3.6, but not in the film Ni–P film plated by ELP-SCE. As it turned out, the ELP-SCE film was entirely free of pinholes, as the hydrogen bubbles produced by the reaction of equation (3) had dissolved in the sc-CO_2

phase distributed in the emulsion.

The film growth rate in ELP-SCE was considerably slower than that in the ELP in the solution alone. This may have been due to the equilibrium reached between the oxidation reaction of the reducing agent and the reduction reaction of the H^+. The H^+ concentration may be supersaturated by dispersed CO_2 in the plating solution during ELP-SCE. Under this condition, the continuous supply of H^+ can be expected to maintain the equilibrium. ELP-SCE was carried out with 30 ml of plating solution, and the reducing made up 12% of the plating solution. The SEM images in Fig. 3.7 show plating films produced by ELP-SCE with different volumes of reducing agent added. Fig. 3.8 shows the film thickness and surface roughness (*Ra*) of plating films produced by ELP-SCE. A higher concentration of reducing agent increases the plating rate.[1] If a film reaches a certain thickness, nodules are prone to form.[9] ELP-SCE, on the other hand, produces a nodule-free film of high smoothness and is generally unaffected by the volume of reducing agent added. The deposition rate in ELP-SCE will not sharply increase when more reducing agent is added, presumably because the plating reaction reaches the equilibrium state described above.

Another point meriting attention is the role of the 3D concentration of H^+ in the H^+-induced suppression of convex, nodule-like portions of the film. Jacobs and Rikken reported a suppression of plating film growth via the nonlinear diffusion

of reactive species to minute convex portions of the film with plating solutions with DO.[11] Fig. 3.9 and equations (7) and (8) can elucidate how the reactive species shielded the nonlinear mass diffusion of the electrtoless deposit. Equations (7) and (8) are the mass flux equations for the species in the electroless plating bath [3,22]

$$J = -\left(\frac{DC_0}{\delta}\right) \tag{7}$$

$$J' = -\left(\frac{DC_0}{\delta} + \frac{4DC_0}{\pi r}\right) \tag{8}$$

where D is the diffusion coefficient, C_0 is the chemical concentration in bulk solution, δ is the thickness of the diffusion layer, and r is the curvature radius of the tiny pattern. Equation (7), equation (8), and Fig. 3.9 describe the diffusion phenomena of reactive species on different microstructures in the ELP bath. Generally, J denotes the mass flux on the panel, J' denotes the mass flux on the tiny substrates (such as nanoparticles or minute convex portions like nodules). When $r \gg \delta$, the species will diffuse as if on a large flat surface and J' will be equal to J. Hence, the diffusion flux J' will be equal to J and will result in linear diffusion, as seen in Fig. 3.9. If, on the other hand, the radius r is so small that the reactive species behave similarly to those on nanoparticles or at the corners

of the openings in a tiny pattern, as shown in Fig. 3.9, the diffusion flux *J'* will be larger than *J* and will result in a nonlinear diffusion. From this viewpoint, the DO was adsorbed more on the minute convex portions of the film than on the plate portions, and it suppressed metal deposition on the portions where it was more adsorbed. The DO confers only a minimal effect in ELP-SCE, however, as it completely dissolves in the dispersed CO_2 phase of the emulsion. Meanwhile, there have been no earlier data on the force driving the diffusion of the DO to minute, convex portions of the film. Judging from the evidence, the nonlinear diffusion of H^+ to nodules is probably driven by the concentration diffusion generated by the consumption of H^+ via the hydrogen gas generation reaction of equation (3).

3.3.5. *Effects of Factors in Different Combinations*

In the next experiments we confirmed the influence of nodule formation on the plating film under variable conditions, with the factors combined in different ways. First, a surfactant was added to the basic plating solution (pH 5.3) used for the conventional method. The SEM image in Fig. 3.10 (a) shows a sample fabricated with agitation at a stirring speed of 500 rpm (sample 6). The nodule formation was not suppressed in this reaction with high-speed agitation, though these were the same conditions that changed the transport characteristic

of the reactive species during deposition onto the substrate. Fig. 3.10 (b) shows the surface of a sample fabricated in a plating solution of pH 4 at the same agitation speed of 500 rpm (sample 7). The next sample (sample 8) was fabricated under the same plating conditions used for sample 7, but with surfactant added (Fig. 3.10 (c)). Undulation was observed on the surfaces of both plating films. The next sample (sample 9) was fabricated under the same plating conditions used for sample 8, but with an extended reaction time (Fig. 3.11). As Fig. 3.11 shows, some parts of the Cu substrate were exposed and the plating film was incompletely coated over the substrate surface. In the EDX analysis, Ni and P were almost too thin to detect and the film itself was far thinner than the film shown in Fig. 3.5 (b). Meanwhile, the SEM observation revealed undulations and holes in the plated portions.

Nodule and pinhole formation on an ELP film are difficult to suppress by the conventional method, but they are suppressed by ELP-SCE. While the plating conditions for sample 9 had many similarities to ELP-SCE, the formation of the plating film itself was unstable. This shows that ELP-SCE forms reaction regions that permit stable plating growth under a low-pH and high-speed-stirring condition. Ultrafine defects are suppressed in these reaction regions, which enables the formation of a very smooth film. This cannot fully explain why the H^+ concentration in the plating solution in ELP-SCE influences

nodule formation. That is, the transport characteristic of the reactive species onto the substrate are probably completely different in ELP-SCE and the conventional method. In order to clarify it, the method of observing the film growth into a minute convex like nodules is required.

Summary

This chapter has reported experiments to demonstrate the effects of agitation, surfactant, DO, and pH, on Ni–P films obtained in sc-CO_2 emulsion. Agitation, surfactant, and DO did not suppress nodule formation. The Ni–P film obtained by ELP in sc-CO_2 emulsion was extremely uniform, and free from pinholes and nodules. Two features of the sc-CO_2 emulsion prevented defects: the stronger acidic solution attained via the dissolution of CO_2 and the transport properties with the diffusive dense CO_2. The phosphorus concentration and film growth rate were compared between plating films fabricated by two ELP techniques, one in sc-CO_2 emulsion (ELP-SCE) and one in Ni–P electroless solution alone. The phosphorus concentration of the film fabricated by ELP-SCE (22.7 wt %) was far higher than that of the film fabricated by ELP in Ni–P solution alone at pH 4.0–5.3. The film growth rate was lower ELP-SCE than in ELP carried out in Ni–P solution alone at pH 5.3 and 4.0. On this basis, we conclude that the film formation ELP-SCE was influenced by the high-speed agitation and decrease in the oxidation of the reducing agent due to the lower pH.

References

1. G. O. Mallory and J. B. Hajdu, *Electroless Plating: Fundamentals and Applications*, American Electroplaters and Surface Finishers Society, Orlando, FL (1990).
2. W. Sha, X. Wu and K. G. Keong, *Electroless Copper and Nickel-phosphorus Plating: Processing, Characterization and Modeling*, Woodhead Publishing, Cambridge, (2011).
3. M. Paunovic and M. Schlesinger, *Fundamentals of Electrochemical Deposition*, 2nd ed., John Wiley & Sons, Hoboken, NJ (2006).
4. A. A. Tracton, in *Coatings Technology Handbook*, 3nd ed., A. Vakelis, Editor, p. 27-1, CRC Press Taylor & Francis Group, New York (2006).
5. L. B. Freund and S. Suresh, *Thin Film Materials*., Cambridge University Press, Cambridge, (2003).
6. C. Gabrielli, and F. Raulin, J. Appl. Electrochem., **1**, 167 (1971).
7. A. Chiba, H. Haijima, and K. Kobayashi, Surf. Coat. Technol., **169**, 104 (2003).
8. H. Yoshida, M. Sone, H. Wakabayashi, H. Yan, K. Abe, X. T. Tao, A. Mizushima, S. Ichihara, and S. Myata, Thin Solid Films, **446**, 194 (2004).
9. Y. Nakamaru, T. Joya, K. Tashiro, and H. Honma, Hyomen Gijutsu, **60**, 661 (2009).
10. B. H. Chen, L. Hong, Y. Ma, and T. M. Ko, Ind. Eng. Chem. Res, 41, 2668 (2002).

11. J. W. M. Jacobs and J. M. G. Rikken, J. Electrochem. Soc., **135**, 2822 (1988).

12. H. Yan, M. Sone, A. Mizushima, T. Nagai, K. Abe, S. Ichihara, and S. Miyata, Surf. Coat. Technol., **187**, 86 (2004).

13. Y. Ishihara, S. Yamane, H. Yamazaki, and H. Tsuge, J. Electrochem. Soc., **142**, 2352 (1995).

14. P. S. Liss and P. G. Slater, Nature (London), Phys. Sci., **238**, 64 (1972)

15. D. Tromans, Ind. Eng. Chem. Res., **39**, 805 (2000).

16. S. Portier and C. Rochelle, Chem. Geol., **217**, 187 (2005).

17. B. J. Hwang and S. H. Lin, J. Electrochem. Soc., **142**, 3749 (1995).

18. K. L. Toews, R. M. Shroll, and C. M. Wai, Anal. Chem., **67**, 4040 (1995).

19. L. M. Abrantes and J. P. Corriea, J. Electrochem. Soc., **141**, 2356 (1994).

20. M. Matsuoka, S. Ogawa, and C. Iwakura, Hyomen Gijutsu, **42**, 918 (1991).

21. I. Ohno and S. Haruyama, J. Jpn. Inst. Met., **20**, 979 (1981).

22. Y. H. Chou, Y. Sung, Y. M. Liu, N. W. Pu, and M. D. Ger, J. Electrochem. Soc., **155**, D791 (2008).

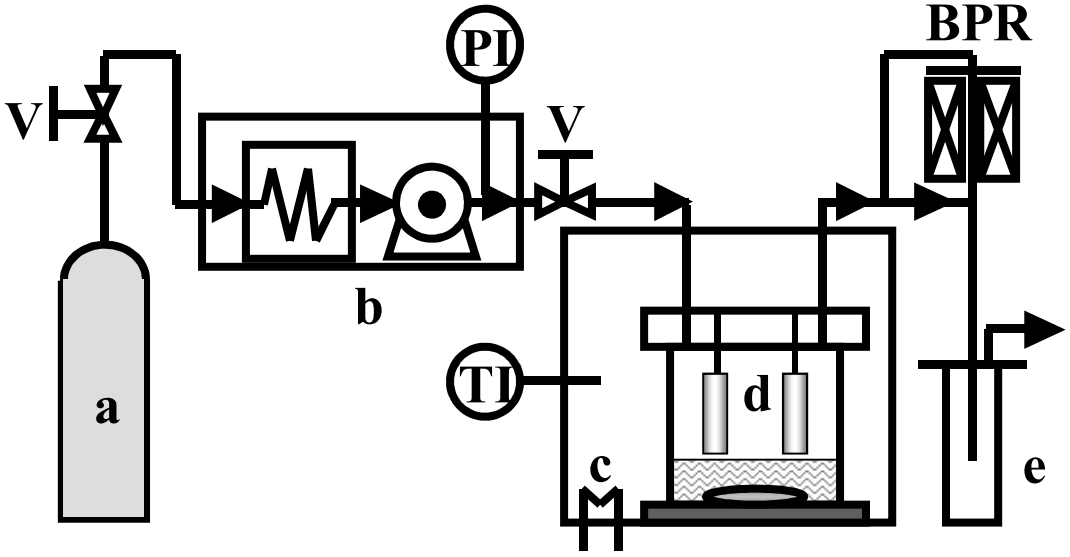

Fig. 3.1 Experimental apparatus used for batch reaction in our electroless plating experiments beyond the critical point of CO_2; (a) CO_2 cylinder; (b) cooler and high pressure pump; (c) temperature controlled air bath; (d) reactor with magnetic stirrer; and (e) trap; BPR: back-pressure regulator; PI: pressure indicator; TI: temperature indicator; V: valves.

Table 3.1. The Properties of the plating film fabricated by ELP-SCE and by electroless plating in the solution alone at different acidities.

Method	pH	Reaction time (min)	Film thickness (μm)	Surface roughness Ra (μm)	Phosphorus content (wt% (atom%))
ELP-SCE	[a]	180	0.80	0.030	22.7 (35.7)
Electroless plating in the solution alone	5.3	5	0.80	0.063	11.3 (19,4)
	4.0	5	0.17	0.023	[b]
		20	0.77	0.027	14.6 (24.5)

[a] Unknown.

[b] Below detection limit of EDX because of the thickness

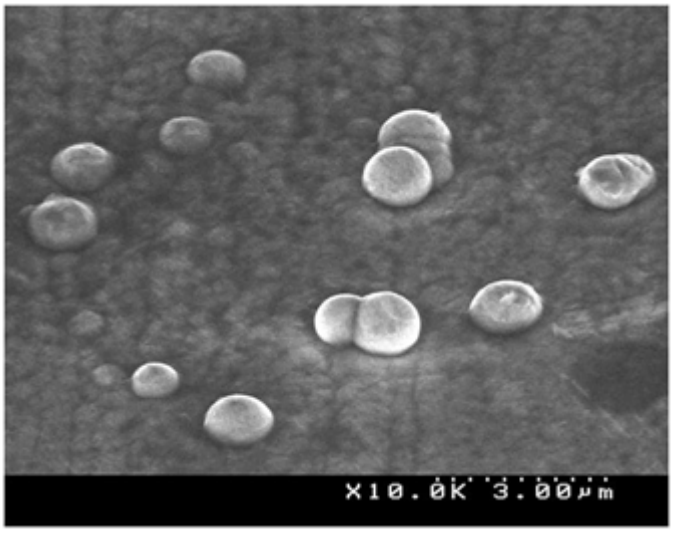

Fig. 3.2 SEM images of Ni-P films plated from electroless plating method in Ni-P electroless plating solution only at 353 K and atmospheric pressure for 5 min and agitation speed is 50 rpm.

Table 3.2. Effect of the agitation speed, the surfactant additive, the dissolved oxygen concentration, and pH on conventional Ni-P plating process.

Sample	Nodule suppression	Reaction time (min)	Agitation speed (rpm)	Surfactant[a]	pH	Surface roughness (Ra) (μm)	SEM image
1	-	5	50	-	5.3	0.063	Fig. 3.2
2	-	5	500	-	5.3	0.032	Fig. 3.3
3	-	5	50	×	5.3	0.035	Fig. 3.4
4	×	5	50	-	4.0	0.023	Fig. 3.5 (a)
5	×	20	50	-	4.0	0.026	Fig. 3.5 (b) and Fig. 3.6
6	-	5	500	×	5.3	0.029	Fig. 3.10 (a)
7	-	5	500	-	4.0	0.031	Fig. 3.10 (b)
8	-	5	500	×	4.0	0.031	Fig. 3.10 (c)
9	-	20	500	×	4.0	0.045	Fig. 3.11

[a] The concentration of surfactant was 1.0 wt % to electroless plating solution.

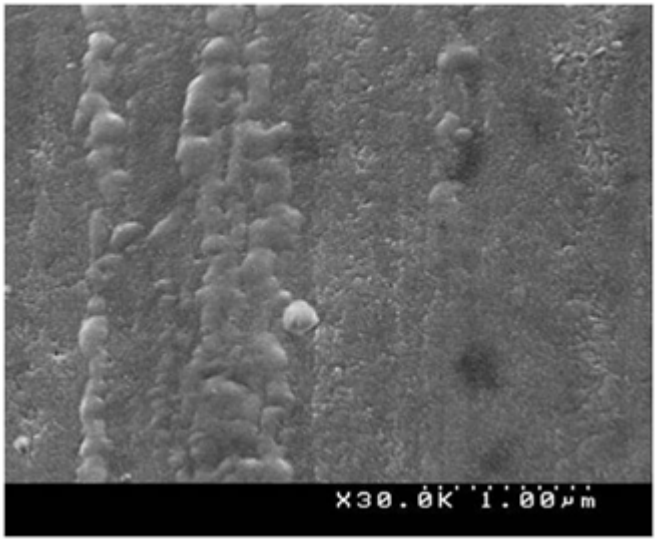

Fig. 3.3 SEM images of Ni-P films plated from electroless plating method in Ni-P electroless plating solution only at 353 K and atmospheric pressure for 5 min and agitation speed is 500rpm.

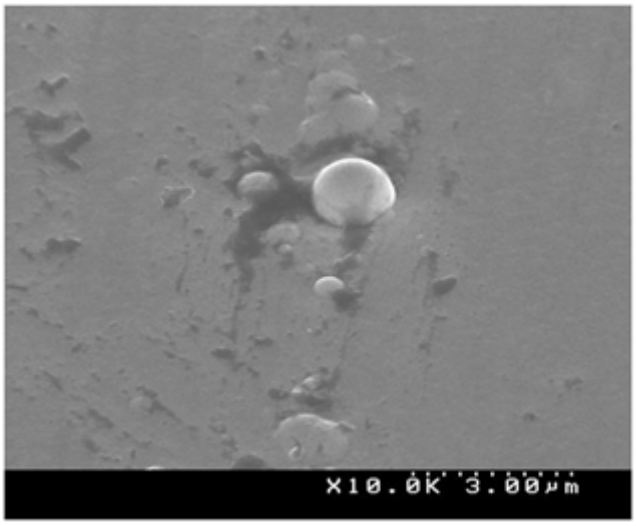

Fig. 3.4 SEM images of Ni-P films plated from electroless plating method in Ni-P electroless plating solution with added nonionic surfactant at 353 K and atmospheric pressure for 5 min and agitation speed is 50 rpm.

Table. 3.3 Dissolved oxygen in electroless Ni-P plating solution added surfactant

	Process				After process	
	Temperature of mixed solution (K)[a]	Pressure (MPa)	Agitation time (min)	Agitation speed (rpm)	DOS (%)[b,c]	Measured temperature of DOS (K)
Condition 1	353	0.1	20	500	84	312
Condition 2	353	15	180	500	68	312

[a] Mixed solution: electroless Ni-P plating solution added surfactant (the concentration of surfactant was 1.0 wt % to electroless plating solution)

[b] DOS: Dissolved oxygen saturation

[c] Dissolved oxygen saturation of the plating solution which carried out air bubbling for 1 hour was set up to 100%.

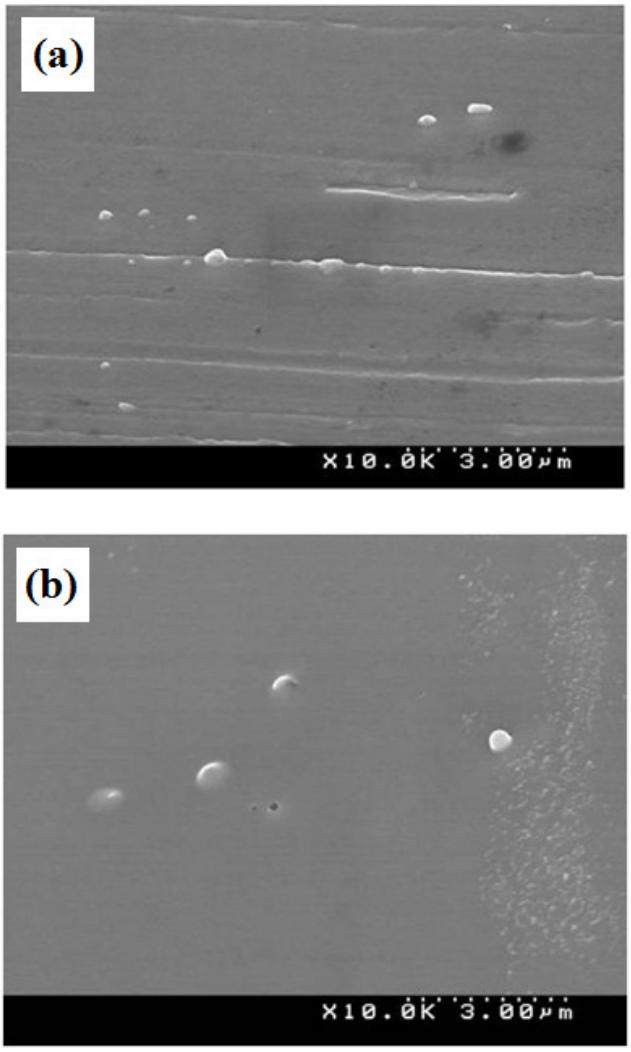

Fig. 3.5 SEM images of Ni-P films plated from conventional electroless plating at 353 K, atmospheric pressure and agitation speed is 50 rpm. (a) reaction time is 5 min and pH of plating solution is 4.0, (b) 20 min, pH = 4.0.

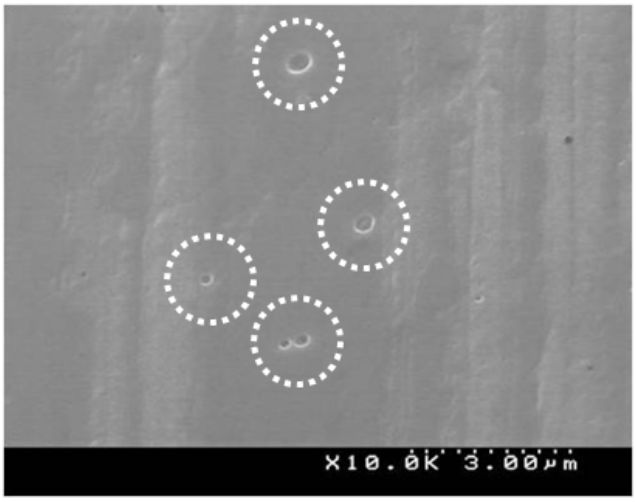

Fig. 3.6 SEM images of Ni-P films plated from electroless plating method in Ni-P electroless plating solution only at 353K and atmospheric pressure (20 min and pH 4.0). White dotted circle shows the pinholes.

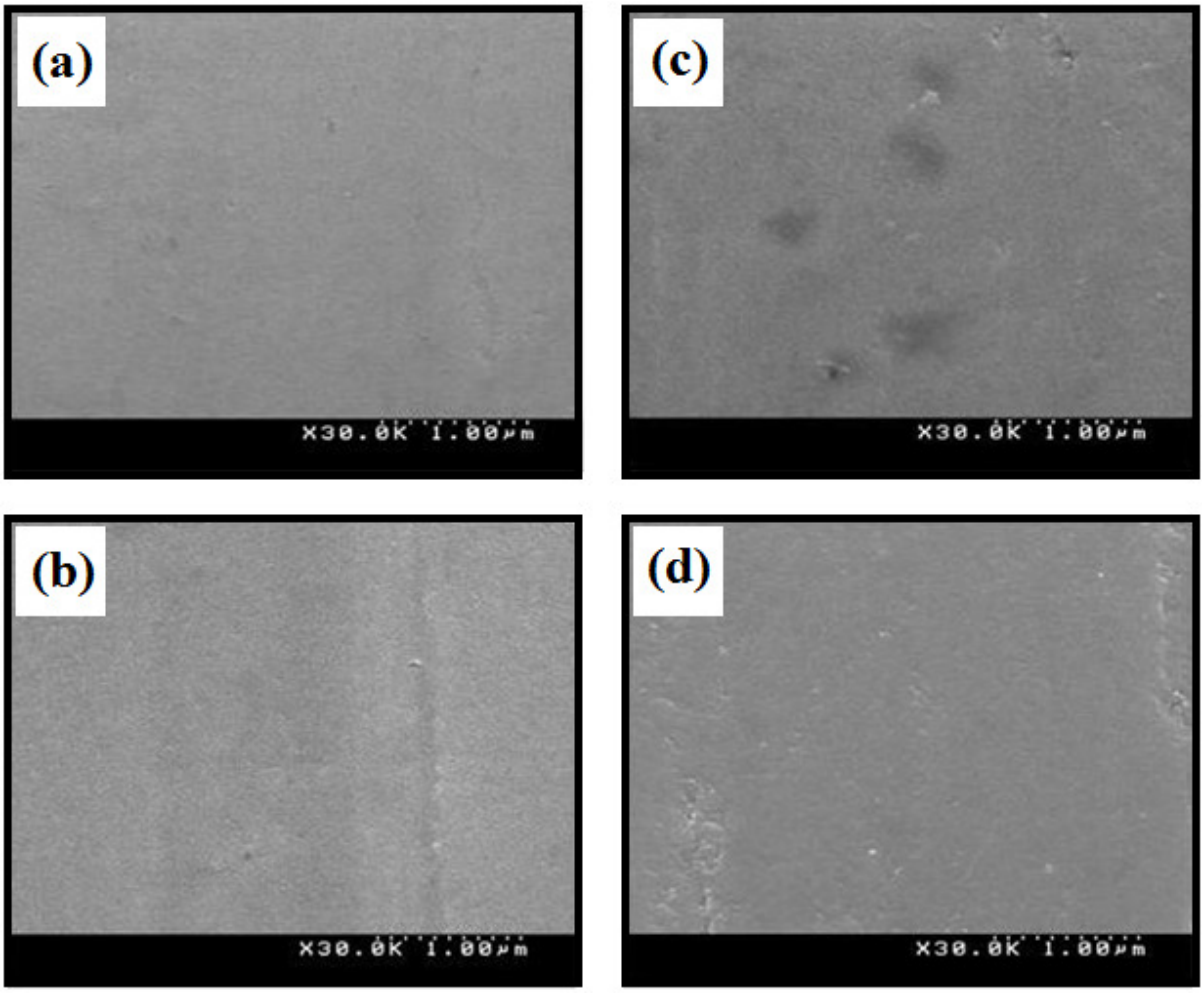

Fig. 3.7 SEM images of Ni–P films plated from ELP-SCE at 353 K and 15 MPa for 180min (a) and with added reducing agent 2g (b), 4g (c), and 6g (d).

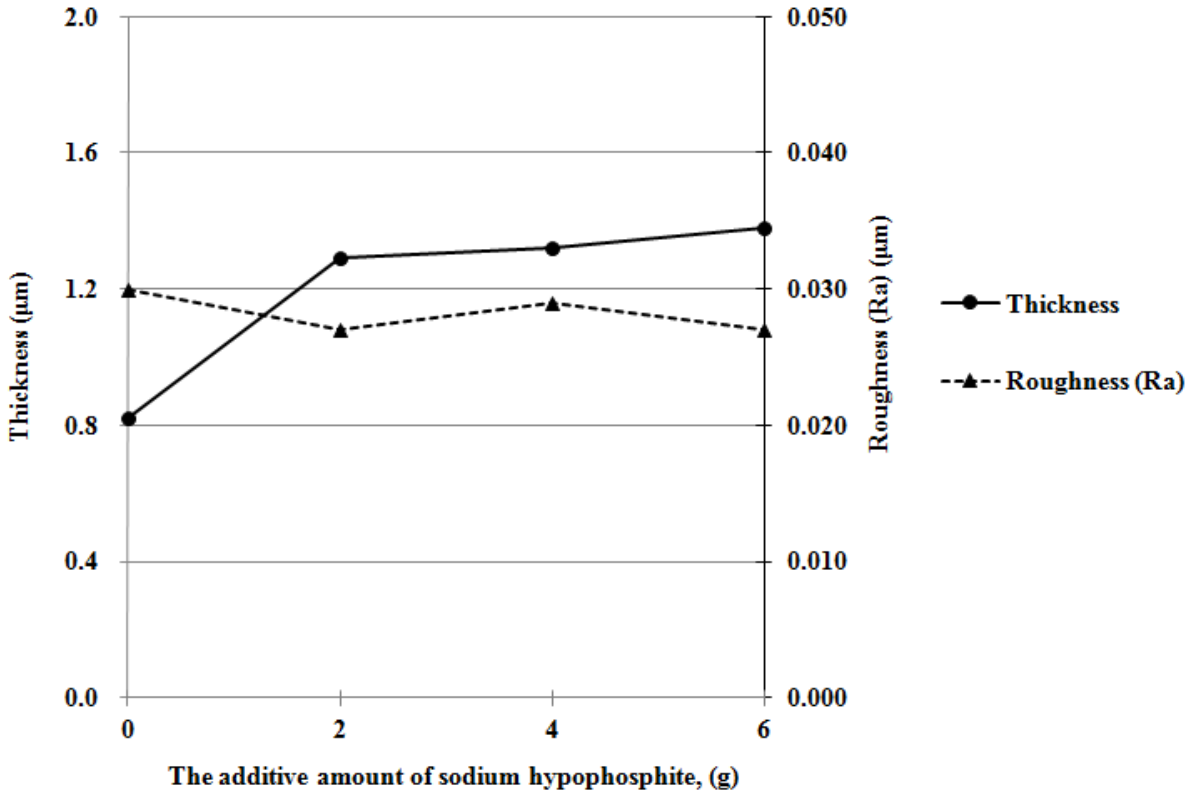

Fig. 3.8 Influence on thickness and surface roughness (Ra) of the Ni-P film made by ELP-SCE to the amount of addition of hypophosphite to the original plating solution. The solid line shows the thickness of the Ni-P film. The dotted line shows the surface roughness of the Ni-P film.

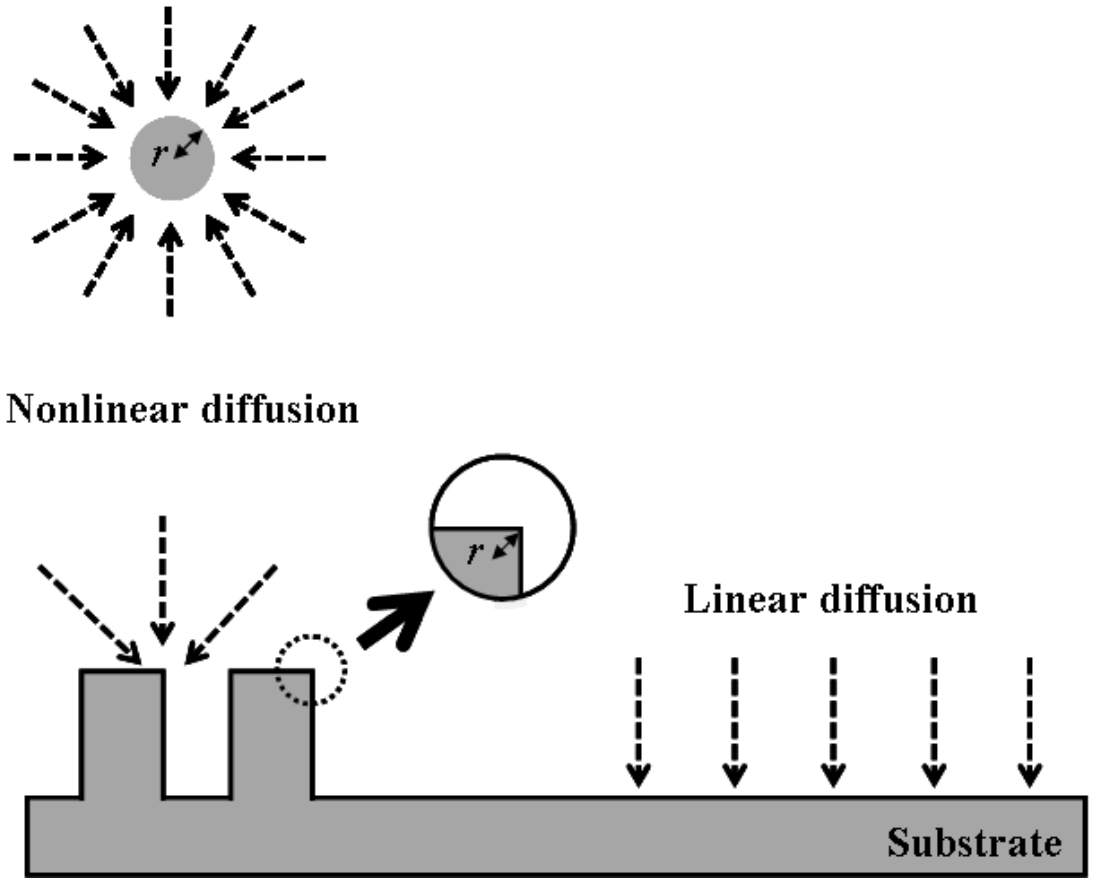

Fig. 3.9 Schematic diagram presenting the diffusion phenomena of chemicals with respect to tiny features of plating substrate.[22]

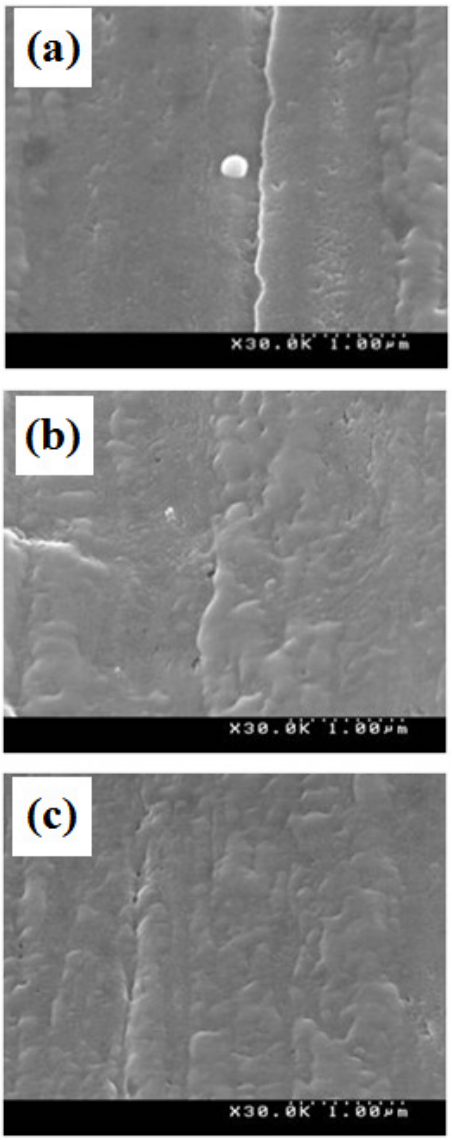

Fig. 3.10 SEM images of Ni-P films plated from conventional electroless plating at 353 K, atmospheric pressure and agitation speed is 500 rpm for 5 min. (a) pH 5.3 with added nonionic surfactant, (b) pH 4.0 without nonionic surfactant, and (c) pH 4.0 with added nonionic surfactant.

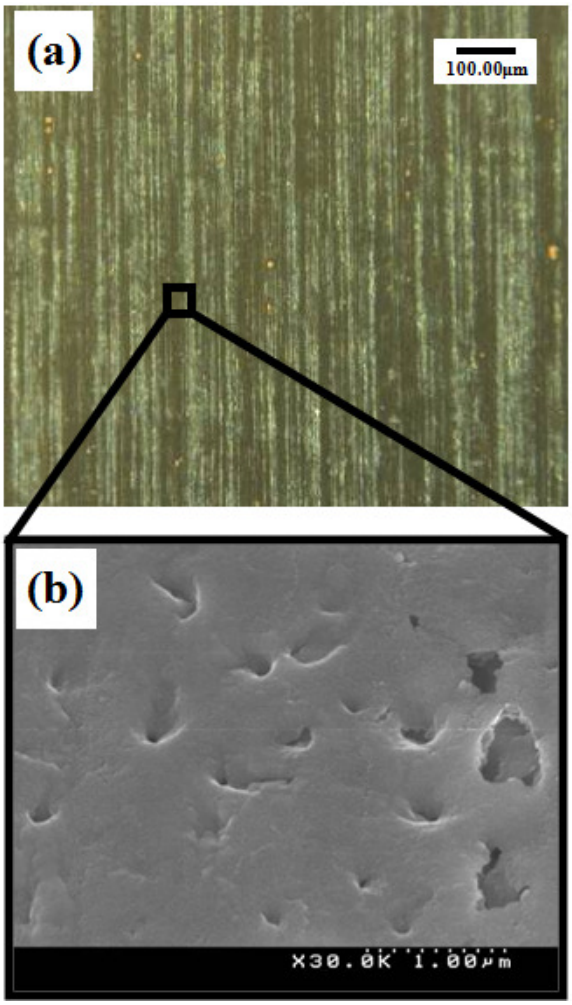

Fig. 3.11 Surface images of Ni–P films plated from electroless plating method in Ni–P electroless plating solution only at 353 K atmospheric pressure and 500 rpm (20 min, pH 4.0, and with added nonionic surfactant): (a) Optical microscopy image and (b) SEM image.

CHAPTER 4

Direct Observation of Nodule Growth on Electroless Ni-P Deposition in Supercritical CO_2 Emulsion

4. 1. Introduction

The plated film obtained by electroless plating using supercritical carbon dioxide emulsion (ELP-SCE) was extremely uniform, smooth and free from pinholes and nodules. The film growth speed of ELP-SCE was slower than the conventional electroless plating (ELP). It is reported that an effect of pulse electroplating-like mechanism by adsorption and desorption of the supercritical CO_2 (sc-CO_2) phase from the plated film, called as "Periodic-Plating-Characteristic (PPC)" is a cause in the smoothing mechanism of the electroplating using a supercritical carbon dioxide emulsion (EP-SCE).[1] PPC might not be the only cause of film smoothing and nodule suppression in ELP-SCE since the film formation mechanisms of electroplating and ELP are

different, though the nodule formation of ELP-SCE can be affected by fast cycle of adsorption and desorption of dispersed carbon dioxide (CO_2) phases to a minute convex part, and for the growth to be suppressed.

In addition, PPC effect itself cannot completely explain the effect of higher P content in Ni-P film by ELP-SCE, and the film growth speed is slower than conventional ELP. As one of the factors of the phenomenon of ELP-SCE, CO_2 dissolves in the plating solution and causes decrease of the pH. When the pH of the plating solution decreases, it is expected to cause P content to increase in the plated film and decrease in the film growth speed.[2] Thus, in previous chapter we discussed that the increase of the proton concentration in the plating solution caused the effect of suppression of nodule growth. However, it is necessary to clarify not only by an indirect method of observing the surface of the plated film via SEM or AFM, but also a direct method of observing growth of one nodule, in order to discuss the suppression mechanism of nodule growth of ELP-SCE clearly. Moreover, the slow film growth speed of ELP-SCE cannot be explained by only making a low pH plating solution. When a plated film fabricated by ELP in the pH=4.0 solution alone with agitation at the same speed used in ELP-SCE, the formation of the plated film was insufficient. For ELP-SCE, the sc-CO_2 phase distributed in the plating solution causes viscosity of plating solution to be low, and, as a result, plating under a high-speed agitation

was enabled. This means thickness of diffusion layer close to surface of substrate and transport property of reactive materials at surface of substrate for ELP-SCE is different from conventional method.

In this study, we discuss what influences the characteristic reaction field of ELP-SCE to the plated film growth. In addition, a novel direct observation of nodule is proposed to clarify the nodule suppression mechanism of ELP-SCE. At first, the Ni-P plated film is plated on Cu substrate by the conventional ELP method, and then re-plating by ELP-SCE or conventional ELP method is conducted on the Ni-P plated film in which nodules were formed by conventional ELP. Moreover, morphology of the nodules at a selected position in the Ni-P plated film is compared before and after the re-plating.

4.2. Experimental method

Base Ni-P (BNP) film preparation for direct observation of nodule

The substrate was a film of 99.99% pure copper measuring 10×20 mm (Mitsubishi Shindoh Co., Ltd.).

The plated film was made by using the ELP solution shown in Table 4.1 at temperature 353K and reaction time 5 minutes. Process procedures from step 1 to step 8 (Pretreatment-A) was shown in Table 4.2. The activation agent, the degreasing agent and the ELP solution were purchased from the Okuno Chemical Co., Ltd. The plating solution was kept in a glass beaker in a temperature-controlled water bath agitated with a magnetic agitator and a cross-magnetic stirrer bar. Agitation speed was 50 rpm. The substrate was inserted to the beaker by stainless steel wires. A lot of nodules were formed on the surface for the plated film made with this condition, and the phosphorus content was 14wt% (Fig.4.1). The plated film is amorphous in as deposited condition and strongly support the observations made from X-ray diffraction (XRD) measurements (Fig.4.2). When plating was performed again, influence from the substrates is a little because it is an amorphous plated film. Thereafter, the Ni-P film made under this process condition is called base Ni-P film (BNP film).

A rectangular shape shown in Fig. 4.3 was fabricated by focused ion beam system (FIB) (accelerating voltage 40kV) on the surface of BNP film. The fabricating area was made by four rectangles of 50×20 μm to make a square observation area of 50×50 μm. The fabrication program was set so that the gallium (Ga) ion beam was not irradiated to the observation area to prevent influence from irradiated Ga ion of FIB to the plated Ni-P film growth at the observation area. The observation area was measured by atomic force microscopy (AFM) before re-plating, and nodules that become observation candidates were decided on the observation area.

The activation treatment using Pd has a big influence on the surface morphology of plated film. This is undesirable to observe the morphological change of the fine nodules.[3] In this study, a pretreatment for the re-plating on the rectangular shaped BNP film was processed in order from step 1 to 6 of Table 4.2 (Pretreatment-B). In the result of the surface texture measuring instrument, Ra of the plated film was 0.029 μm before and after the pretreatment-B, and the AFM measurement result did not have a substantial change in the surface morphology either (Fig. 4.4).

ELP-SCE on pretreated BNP film and on pretreated copper substrate

The rectangular shaped BNP film after pretreatment-B was plated by the conventional ELP and ELP-SCE again respectively. The conventional ELP was the same as the fabrication condition of BNP film. Details on the apparatus and plating method of ELP-SCE can be found in previous chapter (Fig. 4.5). The observation area after re-plating was measured by AFM, and morphology change of the nodule was analyzed. For re-plating, not only rectangular shaped BNP film after pretreatment-B but also the copper substrate after pretreatment-A was performed regardless of each plating method.

Material characterization

Focused ion beam system (FIB, FB-2100, Hitachi High-technologies Co., Ltd.) has scanning ion microscope (SIM). The liquid-metal ion sources of this instrument used Ga ion sources. SIM was used to observe the surfaces of the plated Ni-P films. A cross section of the plated Ni-P film was fabricated by FIB and the thickness of the plated film could be measured directly from the SIM image on the screen. Moreover, FIB was used for fabricating of the area for carrying out direct observation of the nodule growth. The phosphorous composition of the base film was measured by an FESEM (S-4300SE, Hitachi

High-technologies Co., Ltd.) equipped for energy-dispersive X-ray spectroscopy (EDX). An accelerating voltage of 20 kV with a collecting time of more than 300 s was applied. The surface morphology of plated film was examined using an atomic force microscopy (AFM, SPA-400, Seiko Instruments., Inc.) with a calibrated 20 μm xy-scan and 10 μm z-scan range PZT-scanner. A surface texture measuring instrument (Surfcom 480A, Tokyo Seimitsu Co., Ltd.) with a diamond-tipped detector (2 μm tip radius) was used to measure the average surface roughness (Ra) to a minimum resolution of 1 nm for height (height measurement range: 80 μm). The average Ra was calculated from measurements at three points. 2θ-ω X-ray diffraction (XRD) analysis was performed at room temperature (RT, 298 K) using a PANalytical X'pert Pro Galaxy system equipped with an X'celerator module. The X-ray source was CuKα, and the tube voltage and the current are 45 kV and 40mA, respectively.

4.3. Results and discussion

4.3.1. Direct Observation of Nodule Growth in Conventional Method

Copper substrate after pretreatment-A performed with the re-plating procedure had 0.8 μm of the plated film thickness, and it showed a lot of nodules as that of the BNP film as shown in Fig. 4.6 (1-a). This means that decomposition of a plating bath did not occur, when re-plating is performed. Film thickness increased from 0.8 μm to 1.7 μm as a result of re-plating on BNP film after pretreatment-B by conventional ELP, and the number of nodules on the surface increased from the initial state as shown in Fig. 4.6 (1-b). It was possible to re-plating on BNP film with Pretreatment-B. Also, surface observation and film thickness of the plating films by the ELP-SCE and the conventional method using the plating solution with adjusted pH were shown in Figs. 4.6 (2-a), (2-b), (3-a), and (3-b). The stability of the plating solutions in each method were also confirmed by the observations of the plated surfaces. The plated film thickness is 0.6 μm, and the film has grown up on the copper substrate after Pretreatment-A set up simultaneously (Fig. 4.6 (2-a)). The film became a smooth film, although there were ditches resulted from the polishing ditches of the copper substrate. The change from initial film thickness of 0.8

μm could not be observed by SIM observation as a result of re-plating on BNP film after Pretreatment-B by ELP-SCE (Fig. 4.6 (2-b)). The phenomenon in Fig. 4.6 (2-b) is not peculiar and it also happens when the Ni-P film is obtained after Pretreatment-B without Pd activation and re-plated with low pH bath. A similar phenomenon was confirmed for the re-plating with conventional electroless plating adjusted to pH=4.0 by adding HCl (10wt%). The film was formed as for the copper substrate after Pretreatment-B (Fig. 4.6 (3-a)) but the film growth was difficult to be confirmed by the SIM observation from Fig. 4.6 (3-b).

The AFM observation of the BNP film fabricated by FIB before and after re-plating with conventional ELP was shown in Fig. 4.7. Before re-plating, the film was measured with AFM while raising the magnification from Fig. 4.7 (1-a) to (1-c), and nodules at a specific position were decided by three places. After re-plating, the change in the morphology of the specific nodule was observed with AFM from Fig. 4.7 (2-a) to (2-c). The height of nodule before re-plating was 40 nm or less, and the width was about 500 nm. The measurement of the width of nodule was conducted along the direction of the dotted line arrow along the ditch in Fig. 4.7 (1-d) and (2-d). The height of nodules after re-plating decreased by several nm, and the width increased data was summarized in Table 4.3. The shape of nodule was not changed as the film thickness

increased to twice that of the initial thickness. The prior growth of nodules can be considered to come from spherical diffusion layer surrounding the neighboring nodule cores on the surface. The localized concentration by spherical diffusion occurs at the convex part when the thickness of the diffusion layer is the same or thicker than that of the convex part on the surface, and the thickness of the diffusion layer in neighborhood on the plated film greatly influences the surface-roughness of the plated film.[4,5] The thickness of typical Nernst diffusion layer was reported to be about 0.2 mm, and thickness could be about 0.02 mm when agitation is added.[4] In this experimental condition, it was considered that the Nernst diffusion layer was larger than enough to the size of these nodules in resulting the spherical diffusion[6], and led to a surface morphology like Fig. 4.7 (2-d). Moreover, this evaluating method is an effective direct observation method to study the growth mechanism and the surface morphology of the plated film including nodule at a specific position.

4.3.2. Suppression of Nodule Growth in ELP-SCE

An extraordinary effect was confirmed for the morphological change of nodule (Fig. 4.8, Table 4.4). This is the first report on of direct observation of the effect of nodule growth suppression by ELP-SCE. Decrease in size of nodules and initiation of nucleation on the surface at random were observed though the plated film as the film grew up. The ditch parts were on the substrate before re-plating, which were filled after re-plating as shown in Fig.4.8. Random generation of the refined nucleus and leveling effect are similar to the phenomenon that happens because of PPC.[1] The effect of the leveling of ELP-SCE could be caused by the fact that the thickness of the diffusion layer is as thin as the size of these nodules. On the other hand, we discussed the influence of the proton for the growth suppression of nodule in the previous chapter. The re-plating experiment was done by conventional ELP that used the plating bath with pH adjusted to 4.0 by adding HCl (10 wt%) to confirm the influence of diffusion layer thickness of ELP-SCE and the proton. New nodules were observed to be hardly formed after re-plating as shown in Fig. 4.9. The plated film was observed to be from 183 nm to 254 nm as a result of measuring the width of ditch before and after re-plating, because of this re-plating (Fig. 4.9). The height of nodules was several nm against the film growth of about tens of nm though the size of nodule had expanded from Table 4.5. The growth of the

convex part was suppressed under a plating condition even when it was thought that there was a thicker diffusion layer where spherical diffusion happened. However, all peculiar phenomena of ELP-SCE were not able to be shown. That is, the thickness change in the diffusion layer in addition to the influence of the proton greatly influences in ELP-SCE.

The effect of PPC proposed with EP-SCE and the mechanical agitation are the causes for decrease in the thickness of the diffusion layer of ELP-SCE. PPC for the sc-CO_2 phase to repeat adsorption and desorption on the surface of the plated film could appear as similar as that of the pulse electro deposition (PED).[7] Actually, Rahman have succeeded by using the effect of PPC in the sc-CO_2 emulsion and the perfluorocarbon surfactant in forming the porous film.[8] Size of the pores are roughly several μm or less depends on the size of the sc-CO_2 phase, which can be controlled by pressure, the amount of CO_2, and the amount of the surfactant.[1] Moreover, the influence of the mechanical agitation is an important factor in the diffusion layer control. In the PED, the mechanical agitation and the duty cycle are optimized, and the thickness of the diffusion layer is controlled.[9] In ELP-SCE, the plating reaction field is made by making sc-CO_2 and the plating solution in an emulsion to lowered the viscosity. This gives the possibility to exert a difference in influence from the mechanical agitation like the conventional on the growth of the plated film.

Two influences mentioned above on the plating reaction field might be the formation factors of the refined nuclei observed. In the PED, the nucleation is promoted because the plating reaction can be performed at high overpotential, and it becomes easy for a minute crystallization to occur. On the other hand, the ELP that was not applied by the external power is the base reaction in ELP-SCE, and the electron necessary for the nucleation is only supplied by the reducing agent oxidized on the plated film. Also, crystallization overpotential that is higher than nuclear growth are necessary for the nucleation in the electrocrystallization.[10] Therefore, it will be necessary to supply a large amount of reducing agents to a reaction surface in ELP-SCE. The small film growth speed of ELP-SCE might have been caused by the reaction filed where the nucleation occur more frequently than nuclear growth. It causes high P content with plated film by ELP-SCE, moreover, because not only the reducing agent but also other reactive species such as the metal ions and protons are supplied easily voluminously so far because of PPC and the mechanical agitation.

Summary

We examined a direct observation of selected nodule growth in ELP reaction using AFM on a square sample substrate of 50×50 μm fabricated by FIB. The Ni-P plated film is plated by the conventional method and ELP-SCE again on the Ni-P plated film with nodule formed. Changes in fine nodules and other areas at a specific position in the surface morphology were compared before and after the re-plating. In ELP-SCE, the dominant growth of nodules was suppressed and the nucleation occurred on the other surface of the nodules, although the convex part of nodules grew dominantly in conventional ELP using the electrolyte only.

References

1. T. F. M. Chang and M. Sone, *Surf. Coat. Technol.*, **205**, 3890 (2011).
2. G. O. Malloy and J. B. Hajdu, *Electroless Plating: Fundamentals and Applications*, American Electroplaters and Surface Finishers Society, Orlando, FL (1990).
3. T. Tsunoda, H. Nagashima, H. Nishinakayama, H. Watanabe, and H. Honma, *Hyomen Gijutsu*, **56**, 463 (2005).
4. M. Paunovic and M. Schlesinger, *Fundamentals of Electrochemical Deposition*, 2nd ed., John Wiley & Sons, Hoboken, NJ (2006).
5. A. R. Despic and K. I. Popov, *J. Appl. Electrochem.*, **1**, 275 (1971).
6. Y. H. Chou, Y. Sung, Y. M. Liu, N. W. Pu, and M. D. Ger, *J. Electrochem. Soc.*, **155**, D791 (2008).
7. M. S. Chandrasekar and M. Pushpavanam, *Electrochim. Acta.*, **53**, 3313 (2008).
8. Md. Rahman, M. Sone, H. Uchiyama, M. Sakurai, S. Miyata, T. Nagai, Y. Higo, and H, Kameyama, *Surf. Coat. Technol.*, **201**, 7513 (2007).
9. T. L. Lam, A. Koike, I. Ohno, and S. Haruyama*, J. Met. Finish. Soc. Jpn.*, **34**, 428 (1983).
10. R. Kaishev and B. Mutaftschiev, *Electrochim. Acta.*, **10**, 643 (1965).

Table 4.1 Bath composition and operating conditions of electroless Ni-P films

Chemicals	
Nickel chloride	9.0%
Sodium hyphosphite	12.0%
Complexing agent	12.0%
Ion-exchange water	67.0%
pH	5.3
Bath temperature	353K

Table 4.2 Composition of solutions and operating of catalyzing process

Step		Solution composition	Temperature (K)	Duration (min)
1	Cleaning-1	Acetone with ultrasonic cleaning	298	15
2	Cleaning-2	Deionized water	298	1
3	Degreasing	Sodium metasilicate (91.0%)	323	1
		Sodium alkylbenzene sulphonate (5.1%)		
		Surfactant (3.9%)		
4	Rinsing	Deionized water	298	1
5	Acid solution treatment	HCl (10.0%)	298	1
		Ion-exchanged water (90.0%)		
6	Rinsing	Deionized water	298	1
7	Activation	Hydrogen chloride (18.0%)	303	1
		Palladium chloride (0.04%)		
		Ion-exchanged water (81.96%)		
8	Rinsing	Deionized water	298	1

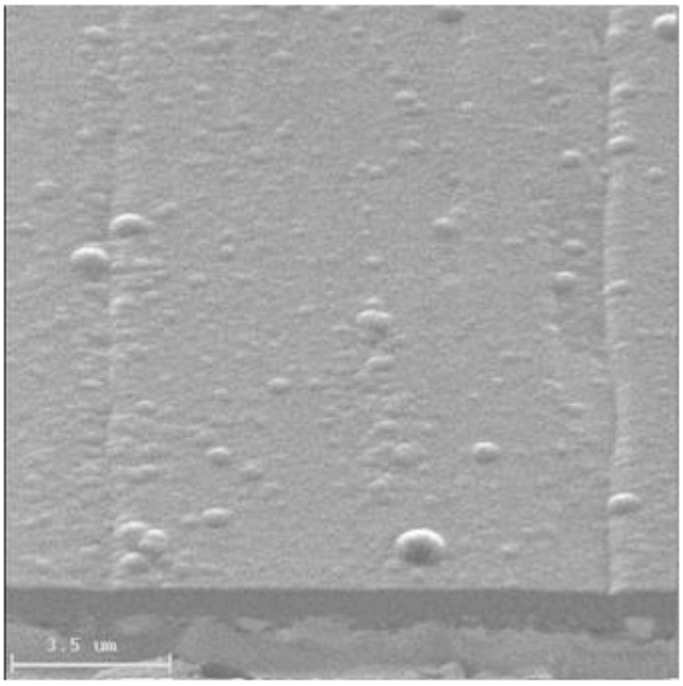

Fig. 4.1 SIM image of Ni-P film by conventional elecroless plating method at 353 K and atmospheric pressure for 5min (with a film thickness of 0.8 μm).

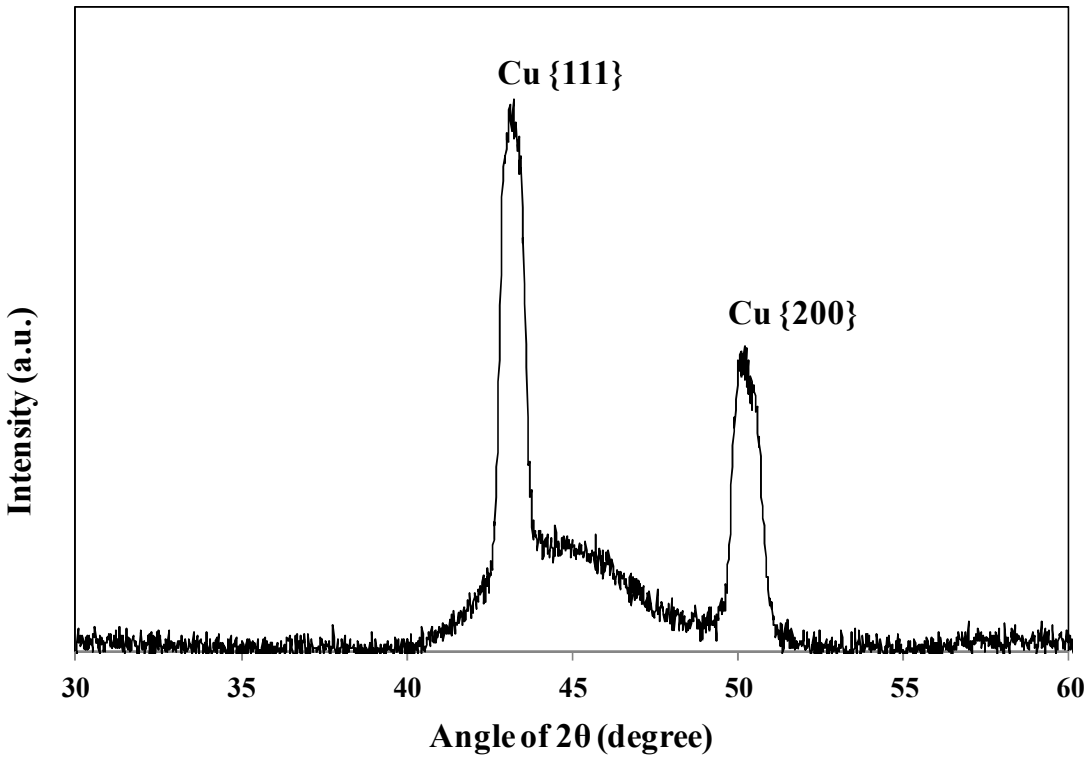

Fig. 4.2 XRD spectrum of Ni-P film plated from conventional electroless plating at 353K and atmospheric pressure for 5 min.

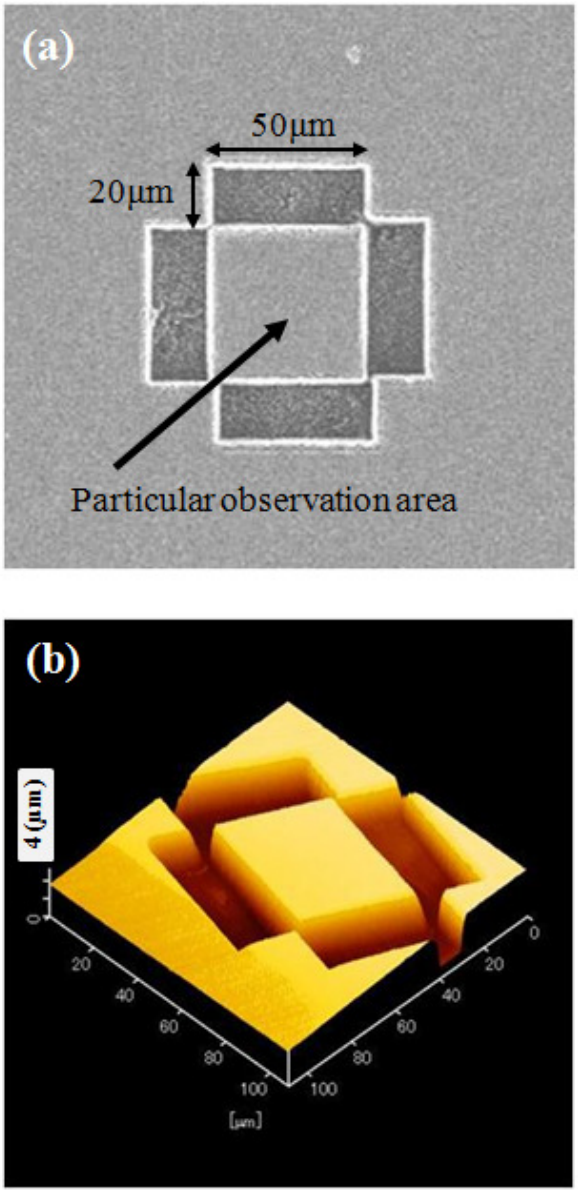

Fig. 4.3 (a) SIM and (b) AFM image of rectangular shaped Ni-P film plated by conventional elecroless plating at 353 K and atmospheric pressure for 5min.

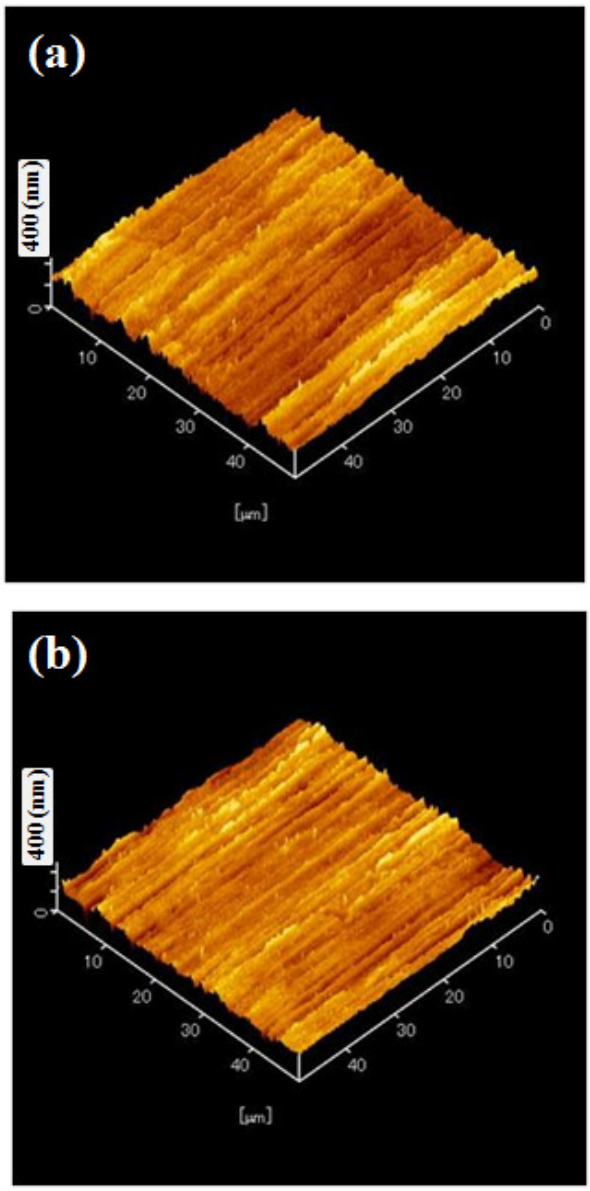

Fig. 4.4 AFM image of (a) Ni-P film by conventional elecroless plating method at 353 K and atmospheric pressure for 5min, and (b) After pretreatment-B.

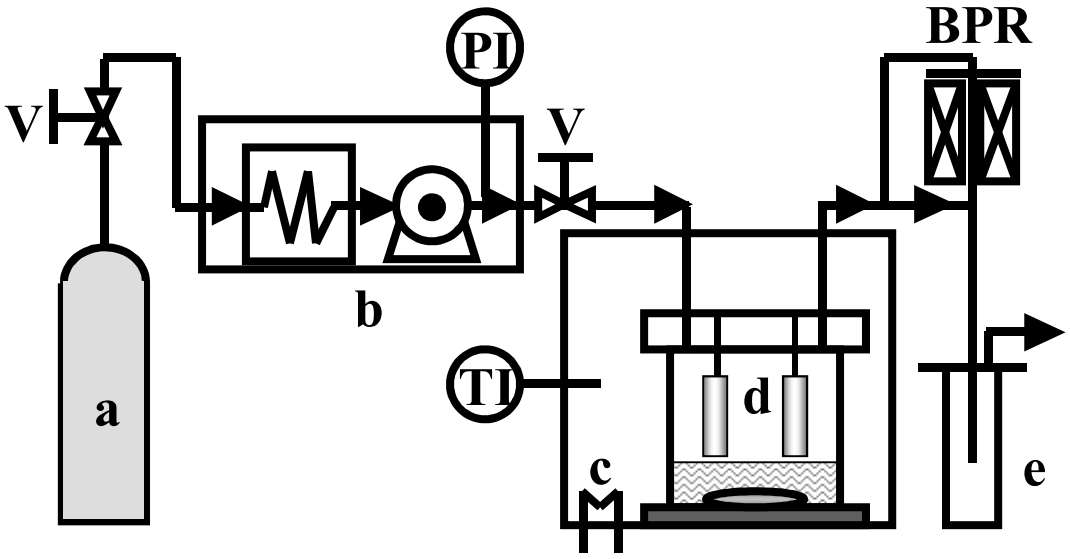

Fig. 4.5 Experimental apparatus used for batch reaction in our electroless plating experiments beyond the critical point of CO_2; (a) CO_2 cylinder; (b) cooler and high pressure pump; (c) temperature controlled air bath; (d) reactor with magnetic stirrer; and (e) trap; BPR: back-pressure regulator; PI: pressure indicator; TI: temperature indicator; V: valves.

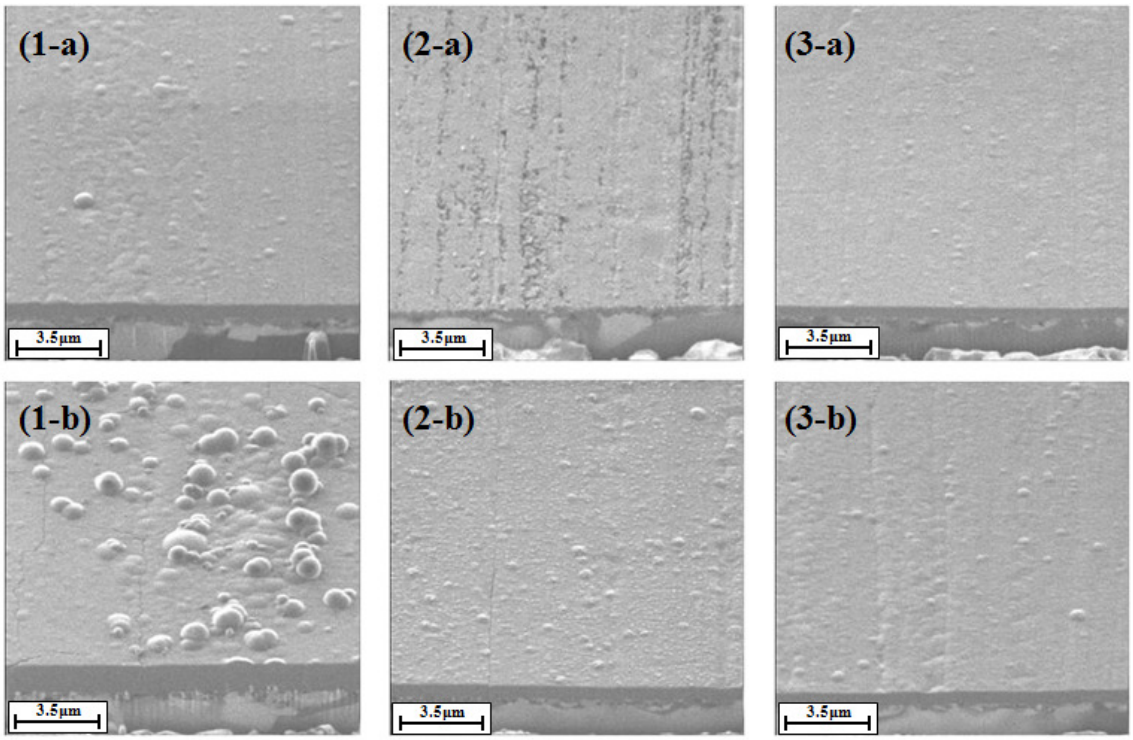

Fig. 4.6 SIM image of Re-Ni-P films plated on the copper substrate by (1-a) conventional elecroless plating method at 353 K and atmospheric pressure for 5 min (with a total film thickness of 0.8 μm), (2-a) ELP-SCE at 353 K and 15MPa for 180 min (with a total film thickness of 0.6 μm) and (3-a) conventional elecroless plating at 353 K and atmospheric pressure for 20 min and pH of plating solution is 4.0 (with a total film thickness of 0.7 μm). (number-b) means SIM image that plates the BNP film being processed for pretreatment-A put at the same time as each (number-a) samples. (1-b) film thickness is 1.7 μm, (2-b) 0.8 μm, (3-b) 0.8 μm.

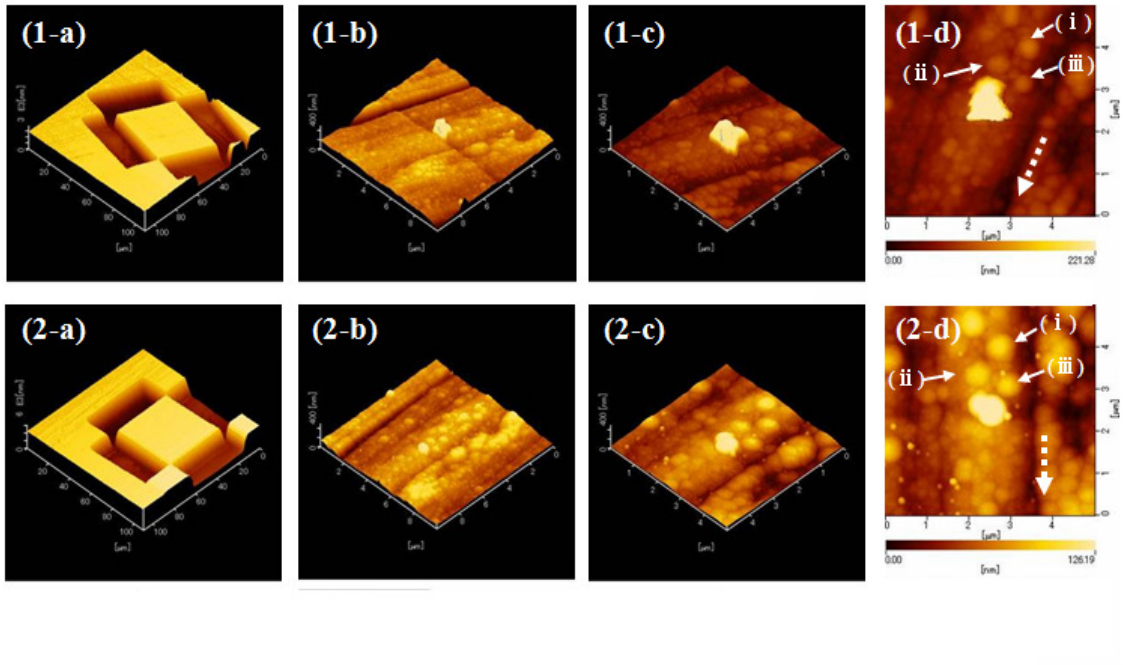

Fig. 4.7 AFM images (1-a, b, c, d) of rectangular shaped Ni-P film plated by conventional elecroless plating method at 353 K and atmospheric pressure for 5 min, and (2-a, b, c, d) of re-plated Ni-P film plated by conventional elecroless plating at 353 K and atmospheric pressure for 5 min on the (1-a) film. The magnification rises from (number-a) to (number-c). (number-d) is 2D image of (number-c). The dotted arrow indicates the direction where the width of nodules was measured.

Table 4.3 Size variation of nodules at particular position before and after re-Ni-P plating from conventional elecroless plating method at 353 K and atmospheric pressure for 5min in Fig. 4.7 (1-d) and (2-d).

	(nm)	Before re-plating	After re-plating	Variation of before and after re-plating
(i)	width	545.8	652.1	+ 106.3
	height	39.1	34.3	- 4.8
(ii)	width	459.4	579.0	+ 119.7
	height	23.5	27.2	- 3.7
(iii)	width	489.4	564.5	+ 75.0
	height	34.2	28.0	- 6.1

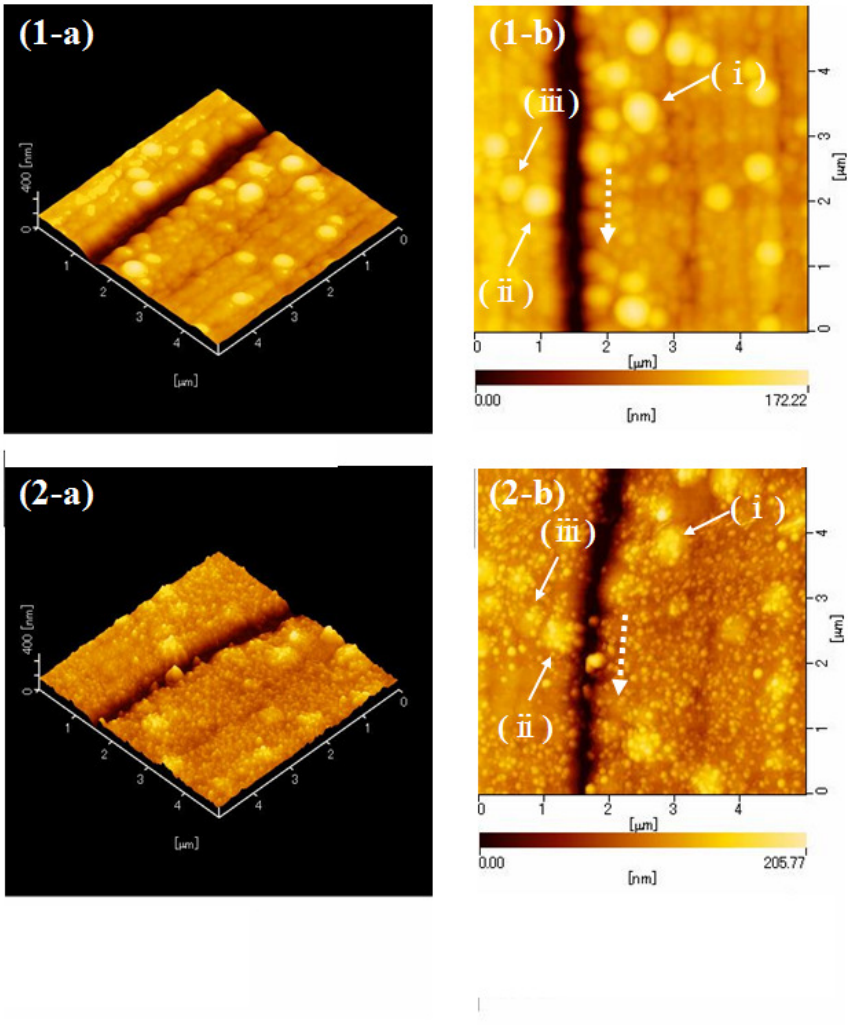

Fig. 4.8 AFM images (1-a) of rectangular shaped Ni-P plating film plated by conventional elecroless plating method at 353 K and atmospheric pressure for 5min, and (2-a) of re-plated Ni-P plating film plated by ELP-SCE at 353 K and 15 MPa for 180 min on the (1-a) film. (number-b) is 2D image of (number-a). The dotted arrow indicates the direction where the width of nodules was measured.

Table 4.4 Size variation of nodules at particular position before and after re-Ni-P plating from ELP-SCE at 353 K and 15MPa for 180min in Fig. 4.8 (1-b) and (2-b)

	(nm)	Before re-plating	After re-plating	Variation of before and after re-plating
(i)	width	603.2	403.6	- 199.6
	height	46.3	36.9	- 9.4
(ii)	width	478.5	419.5	- 59.0
	height	45.4	35.6	- 9.7
(iii)	width	410.6	316.4	- 94.2
	height	33.3	34.0	+ 0.8

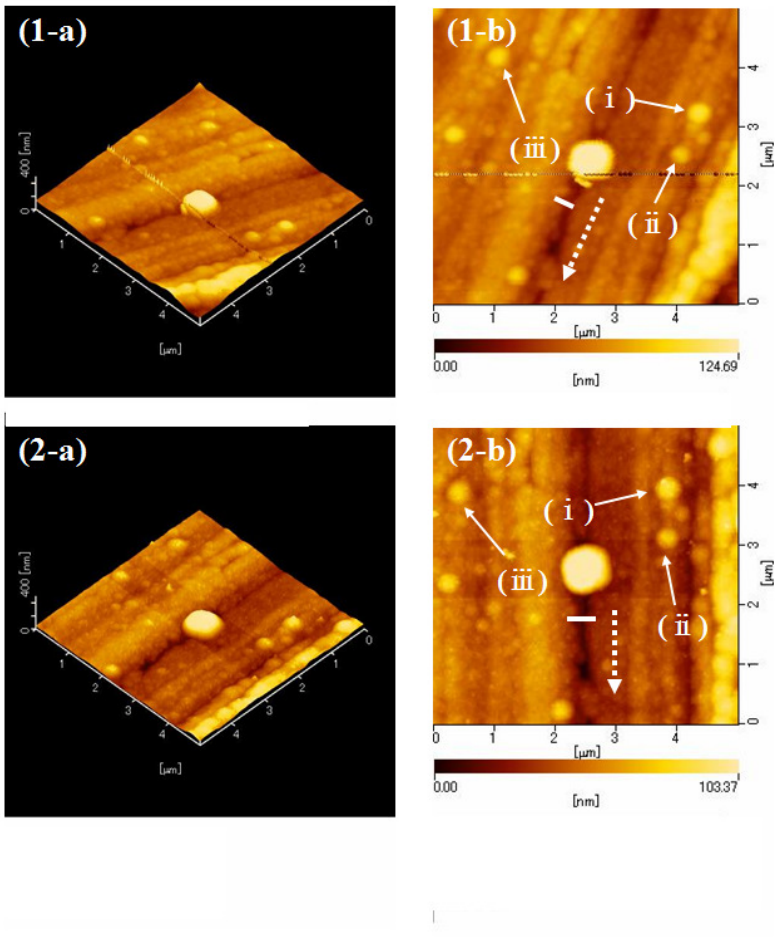

Fig. 4.9 AFM images (1-a) of rectangular shaped Ni-P plating film plated by conventional elecroless plating method at 353 K and atmospheric pressure for 5min, and (2-a) of re-plated Ni-P film plated by conventional electroless plating method at 353 K and atmospheric pressure for 20 min and pH 4.0 of plating solution on the (1-a) film. (number-b) is 2D image of (number-a). The dotted arrow indicates the direction where the width of nodules was measured. Solid line indicates the width of ditch.

Table 4.5 Size variation of nodules at particular position before and after re-Ni-P plating from conventional elecroless plating method at 353 K and atmospheric pressure for 20min and pH of plating solution is 4.0 in Fig. 4.9 (1-d) and (2-d).

	(nm)	Initial	Re-plating	Variation of before and after re-plating
(i)	width	319.5	357.0	+ 37.5
	height	23.3	31.5	+ 8.2
(ii)	width	297.0	321.3	+ 24.3
	height	24.3	28.1	+ 3.8
(iii)	width	394.6	414.2	+ 19.6
	height	24.3	28.1	+ 3.8

CHAPTER 5

Conclusions

In this thesis we proposed a technique for electroless plating using a supercritical carbon dioxide emulsion (ELP-SCE) and comprehensively studied the film-formation and defect-suppression mechanisms of this technique.

In Chapter 2 we proposed a hybrid technique combining electroless plating (ELP) with a supercritical fluid technology. ELP reactions are carried out in an emulsion of supercritical carbon dioxide (sc-CO_2) and an ELP solution with surfactant. Experiments with the proposed technique produced a uniform, high-flatness Ni–P film. This film was free of the pinholes that typically form from the hydrogen bubbles produced by the electrolysis of water, and free of the nodules that typically form from the nuclear growth in the ELP reaction. Pinhole formation was prevented by the dissolution of the hydrogen bubbles in the dense CO_2 particles of the emulsion. We speculate that the nodule formation might have been prevented by the transport properties of the emulsion with the diffusive dense CO_2. The Ni–P film fabricated by our technique was smoother

and more uniform than the pretreated substrate. The roughness of the plated film was constant during film growth, whereas the surface of the film fabricated by conventional ELP tended to roughen as the reaction time increased.

In Chapter 3 we discussed experiments to demonstrate the effects of agitation, surfactant, dissolved oxygen, and pH on the Ni–P film obtained in the sc-CO_2 emulsion. The agitation, surfactant, and dissolved oxygen conferred no effects in suppressing the nodule formation. The density of H^+ in the plating solution was increased by the diffusion and dissolution of CO_2 in the solution, and anomalous growths on the plating film were suppressed. Concurrently, the increased volume of generated hydrogen gas was dissolved in the sc-CO_2 phase distributed in the emulsion. The phosphorus concentration of the film fabricated by ELP-SCE was far larger than that of the film fabricated by conventional ELP at pH 4.0–5.3. The film growth rate was slower in the ELP technique carried out in sc-CO_2 emulsion than in the ELP technique carried out in Ni–P solution alone at pH 4.0-5.3. The film formation in ELP-SCE was influenced by the high-speed agitation and the decrease in the oxidation of the reducing agent due to the lower pH.

In Chapter 4 we proposed a method for directly observing the influence of the ELP-SCE on a nodule and clarified the defect suppression mechanism of ELP-SCE. The Ni-P film was replated by the conventional method and ELP-

SCE on a Ni-P-plated film on which nodules had formed. Changes in fine nodules and other areas at specific positions in the surface morphology were compared before and after the re-plating. The convex part of nodules grew dominantly in conventional ELP using the electrolyte only. Meanwhile the dominant growth of nodules was suppressed and the nucleation occurred on the other surface of the nodules. Random generation of the refined nucleus and leveling effect are similar to that of pulse electroplating, but requires no external power supply. That is, the thickness change in the diffusion layer in addition to the influence of the proton greatly influences in ELP-SCE.

In this thesis we developed an innovative thin film formation method capable of forming thin films with high surface flatness and few defects. Then we elucidated the basic characteristics of the method and the mechanisms by which it suppresses defects such as nodules and pinholes. Finally, we proposed an entirely new electroless plating reaction field. ELP-SCE is an outstanding technology whose strengths in electroless plating outweigh its demerits.

This method can greatly contribute to the development of an integrated, miniaturized 3D device.

Abbreviations

2D	two-dimensional
3D	three-dimensional
AFM	atomic force microscopy
ALD	atomic layer deposition
BNP	base nickel-phosphorus
CFD	chemical fluid deposition
CMOS	complementary metal-oxide-semiconductor
DO	dissolved oxygen
CVD	chemical vapor deposition
Dc-EP	direct current electroplating
EDX	energy dispersive X-ray spectroscopy
ELP	electroless plating
ELP-SCE	electroless plating using a supercritical carbon dioxide emulsion
EP	electroplating
EP-SCE	electroplating using a supercritical carbon dioxide emulsion
FESEM	field emission scanning electron microscope
FIB	focused ion beam
HPLC	high performance liquid chromatography
ICs	integrated circuits
LPCVD	low pressure chemical vapor deposition
MA	metal salt
MEMS	microelectromechanical systems
Ni-P	nickel-phosphorus
Pc	critical pressure
PECVD	plasma enhanced chemical vapor deposition
PED	pulse electro deposition
PPC	Periodic-Plating-Characteristic
Pulse-EP	pulse electroplating
PVD	physical vapor deposition
Red	reducing agent
RESS	rapid expansion of a supercritical solution
Sc-CO_2	supercritical carbon dioxide
SCF	supercritical fluid
SEM	scanning electron microscope
SIM	scanning ion microscope
Tc	critical temperature
XRD	X-ray diffraction

List of Achievement

1. Related Articles

1) "**Uniform Ni-P Film using an Electroless Plating Method with an Emulsion of Supercritical Carbon Dioxide.**" Hiroki Uchiyama, Masato Sone, Chiemi. Ishiyam, and Yakichi. Higo, *Journal of The Electrochemical Society*, **154**, E91 (2007).

2) "**Effects of CO_2 on Ni-P Electroless Plating in an Emulsion of Supercritical CO_2.**" Hiroki Uchiyama, Akinobu Shibata, Masato Sone, and Yakichi. Higo, *Journal of The Electrochemical Society*, **157**, D550 (2010).

3) "**Direct Observation of Nodule Growth on Electroless Ni-P Deposition in Supercritical CO_2 Emulsion.**" Hiroki Uchiyama, Tatsuro Endo, and Masato Sone, *Journal of The Electrochemical Society*, **159**, D114 (2012).

2. Related International Conference Papers

1) "**Uniform Ni-P Film by Electroless Plating Method with the Emulsion of Supercritical Carbon Dioxide.**" Hiroki Uchiyama, Masato Sone, Chiemi. Ishiyam, and Yakichi. Higo, *8th International Symposium on Supercritical Fluids*, 76 (2006).

2) "**Surface Flatness and Interface Stability of Ni-P Film using New Electroless Plating Method with the Emulsion of Supercritical CO_2.**" Hiroki Uchiyama, Masato Sone, Chiemi. Ishiyam, and Yakichi. Higo, *MRS Fall Meeting (Advanced Electronic Packaging)*, **968**, 187 (2006).

2. Related Conference Presentation

1) "**Study on Electroless Ni-P Plating Method using Supercritical Carbon Dioxide**" Hiroki Uchiyama, Masato Sone, Chiemi. Ishiyam, and Yakichi. Higo, *The Society of Chemical Engineers Fall Meeting, Fukuoka*, Japan, Sep. 2006.

2) "**Uniform Ni-P Film by Electroless Plating Method with the Emulsion of Supercritical Carbon Dioxide.**" Hiroki Uchiyama, Masato Sone, Chiemi. Ishiyam, and Yakichi. Higo, *8th International Symposium on*

Supercritical Fluids, Kyoto, Japan, Nov. 2006.

3) "**Surface Flatness and Interface Stability of Ni-P Film using New Electroless Plating Method with the Emulsion of Supercritical CO_2.**" Hiroki Uchiyama, Masato Sone, Chiemi. Ishiyam, and Yakichi. Higo, *MRS Fall Meeting (Advanced Electronic Packaging)*, Boston, USA, Nov. 2006.

4) "**Uniform Metal-Film Fabricated by Novel Electroless Plating Method with an Emulsion of Supercritical Carbon Dioxide.**" Hiroki Uchiyama, Masato Sone, Chiemi. Ishiyam, and Yakichi. Higo, The 1st International Symposium on Supercritical Fluid in Fiber and Textile Science, Funabori, Japan, Jun. 2008.

3. Other Papers

1) "**Novel Porous Film by Electroplating with an Emulsion of Supercritical CO_2.**" Md. Mizanur Rahman, Masato Sone, Hiroki Uchiyama, Makoto Sakurai, Seizo Miyata, Takabumi Nagai, Yakichi Higo, and Hideo Kameyama, *Surface & Coating Technology*, **201**, 7513 (2007).

4. Press

1) **Nikkei Sangyo Shimbun**, Japan, Sep-12, 2006.

Acknowledgements

I would like to express my deep and sincere gratitude to my supervisor, Associate Professor Dr. Masato Sone at Precision and Intelligence Laboratory, Tokyo Institute of Technology. His wide knowledge and his logical way of thinking have been of great value for me. His understanding, encouraging and personal guidance have provided a good basis for the present thesis.

I would like to extend my sincere appreciation to Executive Vice President Professor Dr. Yoshinao Mishima, Professor Dr. Shinji Kumai, Professor Dr. Hideki Hosoda, Associate Professor Dr. Masanori Kajihara, and Associate Professor Dr. Tomoya Inamura at Tokyo Institute of Technology, for their precious instruction, valuable suggestion and encouragement. Especially, I would like to thank Dr. Hosoda and Dr. Inamura for the interesting and fruitful discussions.

I am deeply grateful to Associate Professor Dr. Tatsuro Endo at Osaka Prefecture University, for his valuable advice and friendly help. His extensive discussions have been very helpful for this study.

My warm thanks are due to Emeritus Professor Dr. Yakichi Higo, Emeritus Professor Dr. Kenji Wakashima, Professor Dr. Takeshi Hatsuzawa, Dr. Chiemi Ishiyama at Tokyo Institute of Technology, and Associate Professor Dr Akinobu Shibata at Kyoto University, for their immense instruction and encouragement.

I wish to thank to Ms. Nao Shinoda, Ms. Yuri Shinohara, and Mr. Tso Fu Mark Chang at Tokyo Institute of Technology. Their kind support and guidance have been of great value in this study. My thanks to my friends and colleagues for the great time I had in our group. I enjoyed the atmosphere, their friendship, and their support. It was a pleasure to work with all these people and to benefit from their knowledge.

I would like to thank General Manager Mr. Hidetoshi Shinada, Manager Mr. Tsuyoshi Mita, Manager Mr. Kanji Nagashima, Manager Mr. Yasukazu Nihei, Manager Mr. Yuuichi Okamoto, Manager Dr. Shinji Hikita, Manager Mr. Tomoyuki Takimoto, Mr. Noritoshi Shirai, Mr. Hiroshi Oota, Mr. Tsutomu Yokouchi, Dr. Yoshikazu Hishinuma, Dr. Shinya Sugimoto at FUJIFILM Corporation, Senior Manager Dr. Naoki Morita, Manager Mr. Shigeru Umehara at FUJI XEROX Corporation, and CEO & President Mr. Martin Schoeppler, Vice President Mr. Jeffrey Birkmeyer, Director Dr. Youming Li, Dr. Arman

Hajati, and Mrs. Diane Liu at FUJIFILM Dimatix, Inc..

I gratefully appreciate the financial support of FUJIFILM Corporation and FUJIFILM Dimatix, Inc. that made it possible to complete my thesis.

Finally, I am forever indebted to my family for their understanding, endless patience and encouragement when it was most required.

Hiroki Uchiyama